Effects of blood viscosity fields in hemodynamics and fluid-to-wall mass transport processes in arteries: a mathematical modeling and digital simulation approach

D. Suárez-Bagnasco[1, 2] and R. Suárez-Ántola[1]
[1] Ministry of Industry, Energy and Mines, Montevideo, Uruguay
[2] Faculty of Medicine, CLAEH, Punta del Este, Uruguay

Abstract

Introduction: Both in-vitro and in-vivo observations and experimental research have shown that the radial distribution of red blood cells in blood flowing in arteries is, under certain circumstances, not uniform. Straight segments of small to medium caliber arteries show an axial accumulation of blood cells. A field of apparent variable viscosity appears because of this distribution pattern. Recent research in computational bio-fluid mechanics shows that fluid velocity profiles and wall shear stress in small arteries are affected when the macro-rheological Newtonian and Non-Newtonian blood viscosity mathematical models are compared. Commonly used non-Newtonian models don't consider non-uniform radial distribution of blood cells, and consequently the spatial variation of viscosity. Moreover, variations in shear rates modify fluid-to-wall mass transport processes in arteries, related with the physiology and pathophysiology of arteries.

Objectives: To consider this spatially variable viscosity as it is related to and affects hemodynamics and fluid-to-wall mass transport processes in arteries, emphasizing an approximate analytical approach contrasted with digital simulations.

Materials & methods: One phase incompressible and isotropic theory of viscous suspensions of non-Brownian particles is used to describe blood flow in in straight segments of small arteries. A mathematical model of a spatially variable hematocrit is constructed from given axisymmetric velocity patterns in straight segments of small arteries under quasi-stationary conditions. Velocity profiles, pressures, local viscosity fields, shear rates and wall shear stresses are then obtained using finite elements digital simulation, in straight segments of small arteries under pulsated flow conditions. The effects of the resultant hemodynamics on the parameters of fluid-to-wall mass transport processes are estimated from wall shear rates by means of diffusive boundary layer theory.

Results: In the considered global (tube) haematocrit range (35-55%), obtained shear rate profiles and transport parameters in fluid adjacent to the wall are affected by the macro-rheological model used and by the local haematocrit field according to the micro-rheological model proposed.

Conclusions: Considering spatial variations of viscosity in bio-fluid computational mechanics simulations, may modify significantly local hemodynamics and fluid-to-wall transport processes as well as pumping power needed to maintain pulsated flow in a small artery, both with Newtonian and Non-Newtonian rheology.

Keywords: computational bio-fluid mechanics, rheological models of blood, models of axial accumulation of blood cells, mass transport processes, diffusion boundary layer.

(A) Introduction

Already in the 18th century, Haller and Spallanzani noticed during careful in-vivo observations that blood cells tended to accumulate towards the axis of the vessel. In 1941, Müller observed in-vitro the same behavior, working with a straight capillar tube and a laminar steady flow of a glycerol solution with (same density) suspended micro rubber discs (Taylor 1955; Bayliss 1959). Since 18th century, both in-vitro and in-vivo observations and experimental research have shown that the radial distribution of red blood cells in blood flowing in arteries is often not uniform (Rampling 2007). Besides the always present almost cell-free and slender plasma layer adjacent to the endothelium, there is a variation of the distribution of blood cells inside the lumen of the vessel. The accumulation pattern, if present, depends on the pattern of blood flow.

At first, blood viscosity measurements in cylindrical tube viscometers (with capillary tubes) were done applying Poiseuille formula for a homogeneous Newtonian fluid:

$$\mu = \frac{\pi \cdot R^4 \cdot \Delta P}{8 \cdot L \cdot Q}$$

Here R is tube's radius, L is tube's length, Q is blood flow, and ΔP is pressure difference between tube ends. Tube length L is big enough, so entrance length effects can be neglected.

The viscosity μ should be a blood parameter independent of tube geometry. However, experimental measurements show that there is a relation between apparent viscosity and tube radius. This is the so-called Fahraeus-Lindqvist effect: the apparent viscosity decreases when the tube radius decreases (Ross-Ethier and Simmons 2007; Cokelet and Meiselman 2007a). This gradual decrease in viscosity with decreasing tube size becomes detectable with tubes less than 500µm in internal radius. This reduction becomes significant with tubes less than 200µm in internal radius an up to 50 µm.

There are two classical macro rheological models that explain Fahraeus-Lindqvist effect: wall effect model and sigma effect model.

Wall effect model splits the Newtonian fluid in two phases, a cell free marginal plasma layer, adjacent to the inner wall surface, and a cylinder of uniformly packed red blood cells. Apparent viscosity is given as a function of the quotients between plasma layer thickness (with a thickness of around 3 µm) and tube radius and between plasma viscosity and the viscosity of uniformly packed red blood cell cylinder (Cooney, 1976).

Sigma effect model splits the Newtonian fluid in a finite number of concentric lamina, related to the discrete nature of red blood cells. Each lamina is completely un-sheared internally, and the velocities of adjacent lamina are different. Apparent viscosity is given as a function of plasma viscosity and the quotient between lamina thickness and a uniform whole blood viscosity (Cooney, 1976). Wall effect and sigma effect models are

usually combined to give a more complete formula for the apparent viscosity (Cooney, 1976, Suárez-Ántola, 1980).
Besides, several empirical correlations between blood viscosity, tube radius and global hematocrit were proposed (Baskurt et al. 2007).

Experimental evidence (Pearl, 1961; Cooney, 1976; Baskurt and Meiselman 2007) shows that straight segments of small to medium (from several hundred of µm to mm) caliber arteries present an axial accumulation of blood cells. At low enough shear rates, some of them travel aggregated in rouleaux and others travel free. A field of apparent variable viscosity appears because of this distribution pattern, growing towards vessel axis. To consider this spatial variation, and to make explicit its effect on apparent viscosity, the abovementioned combination of the classical wall effect and sigma effect models is not enough: a different mathematical model must be introduced, even if the fluid is considered as Newtonian. However, below shear rates of about 50 s^{-1} apparent blood viscosity decreases with increasing shear rates (blood thinning), so non-Newtonian rheological models must be used in this case (Cokelet and Meiselman 2007b). Experimental evidence related to the effects of blood cell migration on local viscosities, associated with complex blood flows (related with vessel curvature, ramifications, bifurcations, and changes in cross sections) found in larger vessels (from mm to cm) is fairly scarce. The elucidation of these effects is important because blood viscosity is a key parameter that modulates hemodynamic forces and fluid-to-wall mass transport processes.

One of the main consequences of this modulation is an effect of mechanical transduction at the endothelial level. Endothelial cells that line the inner surface of the artery sense and responds to shear stress. Shear stress patterns affect endothelium permeability and the release of signaling molecules (Nichols et al. 2011). The magnitude and pattern of shear stress are related with the physiology and pathophysiology of arteries (Nichols et al. 2011), and are characterized by several indexes like OSI, WSSG, etc. (Chandran et al. 2012). Moreover, hemodynamics influence fluid-to-wall mass transport processes in arteries and these processes are related also with arterial physiology and pathophysiology, such as atherosclerotic plaque location and development (Ross-Ethier 2002; Tarbell and Qiu 2006; Coppola and Caro 2009; Caro et al. 2012).

Different substances like oxygen and low-density cholesterol (LDL) play a key role in the development and progression of atherosclerotic disease. These substances travel from blood to the artery wall. The transport of some of these substances, like oxygen and other small molecular weight substances may be limited by the convective-dispersive flow from bulk blood to endothelial surface. Between certain bounds, this flow increases with the local fluid shear rate adjacent to the wall. The transport of LDL and other high molecular weight substances seems to be limited mainly by the endothelium. As consequence, as already mentioned above, their flow is modulated by shear stress at the fluid-structure interface.

If blood is modeled as a homogeneous incompressible Newtonian fluid, then shear stress is always proportional to shear rate under any flow conditions. But if flow is modeled as a homogeneous incompressible non-Newtonian fluid, in general the proportionality between shear stress and shear rate vanishes and as consequence mechanical transduction processes doesn´t parallel fluid-to-wall mass transport processes. Recent research in computational bio-fluid mechanics shows that fluid velocity profiles and wall shear stress in small arteries are significantly affected when the Newtonian and the non-Newtonian mathematical models of blood viscosity (for homogeneous fluids without axial accumulation of blood elements or cell free plasma layer) are compared. Kanaris et al. (2012) compared the results of CFD simulations obtained applying a Casson rheological model with the corresponding results obtained with a Newtonian model for a vessel bifurcation. In both cases they considered the dependence of viscosity parameters on the global hematocrit.

If there is a spatially and temporally variable hematocrit field, even in the Newtonian case, without further analysis, the proportionality between shear stress and shear rate should not be taken as granted.

By construction, neither the classical Newtonian nor the commonly used non-Newtonian phenomenological models (like Quemada, Carreau, Bingham, Casson, and Potential Law), consider a possible non-uniform radial distribution of blood cells, and consequently the corresponding spatial variation of viscosity due to particle migration in the flow field (Woodcock 1976, Yilmaz and Gundogdu 2008).

However, to assess the effects of this variable viscosity as it is related to and affects hemodynamics and mass transport processes, it is necessary to consider spatial variation of parameters (mainly due to the migration of blood cells) in blood rheological models used in computational bio-fluid mechanics.

Particle migration is a common phenomenon in flowing suspensions of both, rigid and deformable particles (Davis 1996, Shauly et al. 2000, Scott, 2005, Zhao et al. 2012, van Dinther et al. 2013). In general, migration occurs from regions of high shear rates to regions of low shear rates[1]. This fact can be explained, from a non-equilibrium thermodynamics point of view, applying the principle of minimum entropy production (Quemada 1977, Suárez-Ántola 1980, Glaser 2001, Dillon 2012). While the thermodynamic approach allows an interpretation of particle migration using a common framework, the mechanisms that effectively produce the migration of the suspended particles differ depending on the concentration of the suspension, the size, the shape and the degree of deformability of the suspended particles, buoyancy effects, and flow regime, amongst other properties (Suárez-Ántola 1980).

The main migration mechanism in the case of concentrated suspensions of deformable non-Brownian particles, such as red blood cells, is the so-called hydrodynamic diffusion (Phillips et al. 1992, Davis, 1996, Biasetti et al. 2014). The formula for the suspended particles flux density, derived by Pillips et al. in their phenomenological model of hydrodynamic diffusion, can be re-written (van Dinter et al. 2013) as the product of a positive scalar conductance field by minus the gradient of another scalar field, known as the migration potential. As consequence of this result, suspended non-Brownian particles always move towards regions of lower migration potential. Equilibrium is

---

[1] This remark applies to a dominant population, in the sense that the interaction between its particles and between the carrier fluid and the particles determine the main characteristics of the flow and in particular its energy dissipation. This is the case of the population of red cells in blood. However, the behavior of minority populations, like platelets, white blood cells and eventually drug-delivering particles, may be different and even opposite: instead of migrating towards the conduit axis, the move towards the wall (Baskurt et al. 2007, Zhao et al. 2012).

attained when the migration potential is the same in all points of the fluid.
The conductance field is proportional to the square of the local particle concentration (the local hematocrit if the fluid is blood), the square of a characteristic particle size, and a positive measure of the local shear rate in the fluid. The migration potential field is the logarithm of the product of the local particle concentration, the above-mentioned measure of the local shear rate and a power of the local fluid viscosity.

Recently, Gidaspow and Huang, with the intention of attaining a comprehensive micro rheological theory of Fahraeus-Lindqvist effect, developed a kinetic theory of shear induced particle migration in the framework of a two-phase fluid model for blood flow in narrow straight cylindrical tubes (Gidaspow and Huang 2009).
In this case the migration of the non-Brownian particles towards the axis of the flow is driven by a gradient in a local granular temperature that may be defined for a population of suspended particles in a flow. This temperature decreases radially from the wall to the axis.
Defined as the rate of momentum transfer per unit area due to the interactions between the deforming, translating, and rotating suspended particles, a local collision pressure (roughly proportional to the above-mentioned granular temperature) may be introduced (Suárez-Ántola 1980). This collision pressure (closely related with the migration potential of the hydrodynamic diffusion) appears in a Fokker-Planck equation that approximately describes the time and spatial evolution of the local hematocrit. The spatially variable viscosity of the suspension can be calculated by statistical mechanics methods (Gidaspow and Huang 2009).
As far as the authors know, this kinetic approach has not been applied yet to study migration of deformable particles in complex flows.

Biasetti, Spazzini, Hedin and Gasser (Biasetti et al. 2014) published the results of a CFD research that considers shear induced migration of blood cells in complex flow fields like the ones found in medium to large arteries, working with a non-Newtonian rheological model with realistic values of the global hematocrit. They combined, in single phase non homogenous CFD model, Phillips phenomenological model of hydrodynamic diffusion with Quemada's non-Newtonian phenomenological viscosity model. With the obtained CFD model, an in-silico simulation of the behavior of the formed elements was done: in a normal abdominal aorta, a normal carotid bifurcation, a stenotic carotid bifurcation and an abdominal aneurysm. The results of the digital simulations suggest a significant blood cell migration in the first three cases, but not in the abdominal aneurysm.

(B) Objectives

The general purpose of the present work is to study some aspects of the influence of a spatially variable viscosity on hemodynamics and fluid-to-wall mass transport processes in arteries, using a mixed analytical and numerical framework and **emphasizing the analytical approach**. To ease the application of analytical methods, a simplified model of axisymmetric flow in a straight segment of artery is considered under quasi-stationary conditions, so that the shear stress in the lumen is known and independent of the rheological model.

Under these restrictions, and in the framework of different macro rheological models

(Newtonian, Power Law, Casson, Quemada), our first objective is to characterize spatially variable hematocrits and describe quasi-stationary velocity fields and their associated energy dissipation with approximate analytical methods.
Our second objective is the digital simulation of stationary and pulsated flows, with axial accumulation of blood cells, applying finite elements methods.
Our third objective is to briefly describe the effects of the hemodynamics in the parameters of fluid-to-wall mass transport processes, applying a simplified mathematical model based on diffusive boundary layer theory.

(C) Materials and methods

Blood flow in in straight segments of small arteries is described here by one phase incompressible and isotropic theory of viscous suspensions (Slattery 1972). At each point $\vec{r}$ and instant t, the strain rate tensor $\tilde{\dot{D}}(t,\vec{r})$ and the stress tensor $\tilde{\sigma}(t,\vec{r})$ are given in terms of the fluid velocity field $\vec{u}(t,\vec{r})$, pressure $P(t,\vec{r})$ and the deviatoric stress tensor (extra-stress tensor) $\tilde{\tau}_D(t,\vec{r})$:

$$\tilde{\dot{D}} = \frac{1}{2}\cdot\left(\nabla\vec{u} + \nabla\vec{u}^T\right) \qquad (1) \qquad\qquad \tilde{\sigma} = -P\cdot\tilde{I} + \tilde{\tau}_D \qquad (2)$$

As usual, ∇ represents the gradient operator, $(\ )^T$ the transposition operator and $\tilde{I}$ the unit tensor. Scalar shear stress and strain rate are defined thus (Slattery 1972):

$$\tau = \sqrt{\frac{1}{2}\cdot trace\left(\tilde{\tau}_D \bullet \tilde{\tau}_D\right)} \qquad (3) \qquad\qquad \dot{\gamma} = \sqrt{2\cdot trace\left(\tilde{\dot{D}} \bullet \tilde{\dot{D}}\right)} \qquad (4)$$

A general constitutive equation for blood, considered as an isotropic incompressible fluid with apparent viscosity $\mu(H_t,\dot{\gamma})$ and local hematocrit H_t can be written:

$$\tilde{\tau}_D = 2\cdot\mu(H_t,\dot{\gamma})\cdot\tilde{\dot{D}} \qquad (5)$$

From the scalar shear stress and strain rate, and equation (5), the scalar constitutive equations for an isotropic fluid are obtained:

$$\tau = \mu(H_t,\dot{\gamma})\cdot\dot{\gamma} \qquad (6) \qquad\qquad \dot{\gamma} = \varphi(\tau,H_t)\cdot\tau \qquad (7)$$

If the scalar shear stress and strain rate are known in each point and instant, and if the apparent viscosity is known as a function of the local hematocrit and the scalar shear rate, from (6) it is possible to determine the local hematocrit field $H_t(t,\vec{r})$.

The one phase fluid dynamics equations for an isotropic and incompressible fluid are (being ρ blood density, a volume weighted combination of plasma and cells densities):

$$\rho\cdot\left(\frac{\partial\vec{u}}{\partial t} + \vec{u}\bullet\nabla\vec{u}\right) = -\nabla P + \nabla\cdot\tilde{\tau}_D + \rho\cdot\vec{F} \qquad (8) \qquad\qquad \nabla\bullet\vec{u} = 0 \qquad (9)$$

Neglecting the term due to external forces $\rho \cdot \vec{F}$, from equations (1) and (5) it follows:

$$\rho \cdot \left(\frac{\partial \vec{u}}{\partial t} + \vec{u} \bullet \nabla \vec{u} \right) = -\nabla P + \nabla \cdot \left(\mu(H_t, \dot{\gamma}) \cdot \left[\nabla \vec{u} + \nabla \vec{u}^T \right] \right) \tag{10}$$

The spatial and temporal evolution of the local hematocrit field is given by the continuity equation:

$$\frac{\partial H_t}{\partial t} + \vec{u} \bullet \nabla H_t = -\nabla \bullet \vec{J} \tag{11}$$

Here the vector field $\vec{J}$ represents the flux density of blood cells (mainly red cells) relative to the bulk suspension velocity $\vec{u}$. From a non-equilibrium thermodynamics point of view (Lebon et al. 2010), it can be considered as an internal variable added to the external blood variables ρ, $H_t, \vec{u}$ and T (the assumed uniform temperature of blood).

This one phase continuum approach allows a macroscopic description of red cell migration through the space-time distribution of a macroscopic field of hematocrit. However, it can’t cope with the cell free marginal plasma layer, adjacent to the inner wall surface, which is a microscopic phenomenon relative to scale of the continuum model. So the distribution of the local hematocrit at the wall of the conduit, given by the mathematical model, should be interpreted as the hematocrit at the inner boundary of the cell free plasma layer.

For concentrated suspensions, like blood, the migration of particles may be suitably described by hydrodynamic diffusion theory (Davis, 1996), employing Phillips model (Phillips et al. 1992). As shown in van Dinter et al. (van Dinter et al. 2013), the formula for particle´s migration current density can be re-written as the product of a positive scalar conductance field known as the hydrodynamic diffusion coefficient D_{HD} by minus the gradient ∇ of another scalar field $\Pi(t, \vec{r})$, known as the **migration potential**:

$$\vec{J} = \vec{J}_{HD} = -D_{HD} \cdot \nabla \Pi \tag{12}$$

Here D_{HD} is proportional to the square of the local particle concentration (the local hematocrit H_t if the fluid is blood), the square of a characteristic particle size a, and a positive measure of the local shear rate in the fluid $\dot{\gamma}$:

$$D_{HD} = K_c \cdot H_t^{\,2} \cdot a^2 \cdot \dot{\gamma} \tag{13}$$

The migration potential field is the logarithm of the product of the local particle concentration, the local shear rate measure, and a power of the local fluid viscosity μ:

$$\Pi = \ln\left(H_t \cdot \dot{\gamma} \cdot \mu^{\lambda} \right) \tag{14}$$

Here $\lambda = \dfrac{K_\mu}{K_c}$ is the quotient of two positive non dimensional parameters that take into account friction and electrostatic forces during the interaction of charged particles and are of the order of unity. Streamline curvatures can be incorporated in the migration potential for analytical purposes (Shauly et al. 2000).

From (11) and (12) we obtain:

$$\frac{\partial H_t}{\partial t} + \vec{u} \bullet \nabla H_t = \nabla \bullet \left(D_{HD} \cdot \nabla \Pi \right) \tag{15}$$

Working with equation (14), the following formula for the gradient of the migration potential is derived: $$\nabla\Pi = \left(\frac{1}{H_t} + \lambda \cdot \frac{\partial}{\partial H_t}\ln\mu\right)\cdot\nabla H_t + \left(\frac{1}{\dot\gamma} + \lambda\cdot\frac{\partial}{\partial\dot\gamma}\ln\mu\right)\cdot\nabla\dot\gamma \qquad (16)$$

From (12) and (16) the flux density of suspended particles due to hydrodynamic diffusion can be decomposed in the sum of a convective migration term and a diffusive term: $$\vec{J} = \vec{J}_{HD} = H_t \cdot \vec{u}_m - D\cdot\nabla H_t \qquad (17)$$

The migration velocity $\vec{u}_m$ and the diffusion coefficient D are given by the formulae:

$$\vec{u}_m = -K_c \cdot H_t \cdot a^2 \cdot \left(1 + \lambda\cdot\frac{\partial \ln\mu}{\partial \ln\dot\gamma}\right)\cdot\nabla\dot\gamma \qquad (18)$$

$$D = K_c \cdot H_t \cdot a^2 \cdot \dot\gamma \cdot \left(1 + \lambda\cdot\frac{\partial\ln\mu}{\partial\ln H_t}\right) \qquad (19)$$

For dilute enough suspensions hydrodynamic diffusion ceases to be the main particle migration mechanism. However, although now with a different meaning of the migration velocity $\vec{u}_m$ and the diffusion coefficient D, the particle flux density $\vec{J}$ can be written also as $\vec{J} = H_t \cdot \vec{u}_m - D\cdot\nabla H_t$ (Scott 2005).

From equations (15) and (17) we derive: [2]

$$\frac{\partial H_t}{\partial t} = -\nabla \bullet \left(\left(\vec{u} + \vec{u}_m\right)\cdot H_t\right) + \nabla \bullet \left(D\cdot\nabla H_t\right) \qquad (20)$$

Near the wall, the field of scalar shear strain rate, given by equation (4), influence fluid to wall mass transport in the diffusive boundary layer adjacent to the endothelium (Ross-Ethier 2002). This has particular importance when the limit step to mass transport and reaction is in this diffusive layer, as seems to be the case of oxygen, ATP, bradykinin, angiotensin, and other effectors degraded or chemically modified at the surface of the endothelium (Caro 2001, Tarbell and Qiu 2006). When the chemical species are carried by blood cells, as is the case of oxygen, the lowering of the local hematocrit near the wall, due to axial migration of blood cells, could affect the concentrations of the dissolved substance and decrease fluid to wall mass transport (Biasetti et al. 2014).

(C.1) A framework for a simplified analytical approach

To ease the application of analytical methods, a simplified model of axisymmetric flow in a straight segment of artery is considered under quasi-stationary conditions. Cylindrical coordinates r, θ, z will be used. For transient conditions and a cylindrical conduit with rigid walls, the fluid velocity is parallel to the axis z, equation (5) and (10) reduce to the following (being L the tube length) and $|...|$ the absolute value:

---

[2] Hematocrit kinetics can be described as a continuous random process if the local hematocrit $H_t(t, \vec{r})$ is interpreted as a probability density of finding a red blood cell in each position in a given time instant. By its appearance, equation (20) seems to be closely related with a Fokker-Planck equation (Gardiner 1986). However, its coefficients are functions of the probability density $H_t(t, \vec{r})$.

$$\tau(t,r) = \mu\left(H_t(t,r), \left|\frac{\partial u}{\partial r}(t,r)\right|\right) \cdot \frac{\partial u}{\partial r}(t,r) \qquad (21)$$

$$\rho \cdot \frac{\partial u(t,r)}{\partial t} = \frac{\Delta P(t)}{L} + \frac{1}{r} \cdot \frac{\partial}{\partial r}\left(r \cdot \tau(t,r)\right) \qquad (22)$$

The time varying pressure difference between the inlet and the outlet can be expressed as its maximum ΔP_M multiplied by a suitable function of time: $\Delta P(t) = \Delta P_M \cdot f(t)$ (23)

Now let us consider quasi-steady conditions to calculate the pumping power $\dot{E} = \Delta P \cdot Q$ needed to sustain a given flow Q. Under quasi-steady state conditions, equation (22) simplifies to:

$$\frac{\Delta P(t)}{L} \approx -\frac{1}{r} \cdot \frac{\partial}{\partial r}\left(r \cdot \tau(t,r)\right) \qquad (24)$$

If R is tube radius, let us introduce the dimensionless radial distance: $y = \frac{r}{R}$ (25)

From equation (24), we obtain the (well known) **rheology independent formula for shear stress** (Caro et al. 2012, Chandran et al. 2012):

$$\tau(t,r) \approx \frac{R \cdot \Delta P(t)}{2 \cdot L} \cdot y \qquad (26)$$

To calculate flow as a function of ΔP we begin with the formula for shear rate as a function of shear stress and hematocrit: $\dot{\gamma} = \varphi(\tau, H_t) \cdot \tau = h(\tau, H_t)$

Now $\dot{\gamma}(t,r) = -\frac{\partial u(t,r)}{\partial r} = -\frac{1}{R} \cdot \frac{\partial u(t,y)}{\partial y}$ and $-\frac{\partial u(t,y)}{\partial y} = R \cdot h\left(\frac{R \cdot \Delta P(t)}{2 \cdot L} \cdot y, H_t(t,y)\right)$

Blood flow is given by $Q(t) = \int_0^R 2\pi \cdot r \cdot u(t,r) \cdot dr = 2\pi \cdot R^2 \cdot \int_0^1 y \cdot u(t,y) \cdot dy$. Taking into account the non-slip boundary condition at the wall $u(t, y=1) = 0$ and integrating by parts it follows:

$$Q(t) = \pi \cdot R^3 \cdot \int_0^1 h\left(\frac{R \cdot \Delta P(t)}{2 \cdot L} \cdot y, H_t(t,r)\right) \cdot y^2 \cdot dy \qquad (27)$$

From equation (27), we can derive:

$$\frac{\Delta P}{L} = f(Q,R) \qquad (28)$$

Then we can estimate pumping power to sustain a given blood flow in the conduit:

$$\dot{E} \approx Q \cdot \Delta P = Q \cdot L \cdot f(Q,R) \qquad (29)$$

To be able to use equation (29) it is necessary to determine $\dot{\gamma} = h(\tau, H_t)$ by means of a rheological model that considers the effect of a varying hematocrit. For the present purpose, the validity of the known relations between the parameters of popular models of blood macro rheology (Newtonian, Power Law, Casson, Quemada) and the global hematocrit $H_{t,g}$ is extended to a relation between the local parameters and the local hematocrit H_t. This assumption seems to be a reasonable approximation when the derivation of the relation between the viscosity and global concentrations (Lapasin et al. 1996, Starov et al. 2002, Scott 2005) is re-examined.

The constitutive equations for Newtonian models, with a local viscosity dependent of the local hematocrit (that could be called a **generalized Newtonian models**), are:

$$\tau(t,r) = \mu_N(H_t(t,r)) \cdot \dot{\gamma}(t,r) \tag{30}$$

Here we assume, being μ_p plasma viscosity, $H_{t,M}$ a maximum packing fraction (often taken as 1) and k a dimensionless parameter (often taken as 2):

$$\mu_N(H_t) \approx \frac{\mu_p}{\left(1 - \dfrac{H_t}{H_{t,M}}\right)^k} \tag{31}$$

The non-Newtonian Potential Law model is given by $\tau = \mu_{PL}(H_t, \dot{\gamma}) \cdot \dot{\gamma}$ with an apparent viscosity $\mu_{PL}(H_t, \dot{\gamma}) = K_{PL}(H_t) \cdot \dot{\gamma}^{n-1}$. For blood, to describe shear thinning, the positive parameter n is less than one. It can be derived from a fractal model (Lapasin et al. 1996).

The non-Newtonian Casson model is given by $\tau = \mu_C(H_t, \dot{\gamma}) \cdot \dot{\gamma}$ with an apparent viscosity:

$$\mu_C(H_t, \dot{\gamma}) = \left(\sqrt{\frac{\tau_y(H_t)}{\dot{\gamma}}} + K_c(H_t) \right)^2 \tag{32}$$

When $\tau \le \tau_y$, the shear strain rate is zero. When $\tau > \tau_y$, the shear strain rate is an increasing function of the shear stress. From (32) it follows that if $\dot{\gamma}$ grows without bound, the asymptotic viscosity is $K_c{}^2(H_t) = \mu_N(H_t)$ (Here we suppose that $\mu_N(H_t)$ is given by equation (31)). The yield stress $\tau_y(H_t)$ is an increasing function of the hematocrit. As the hematocrit can vary from place to place and from instant to instant, the yield stress is in general a field $\tau_y(t, \vec{r})$.

The non-Newtonian Quemada's model has a constitutive relation $\tau = \mu_Q(H_t, \dot{\gamma}) \cdot \dot{\gamma}$ with an apparent viscosity (Quemada 1978 (a) and 1978 (b)):

$$\mu_Q(H_t, \dot{\gamma}) = \frac{\mu_p}{\left(1 + \dfrac{[\mu](\dot{\gamma})}{2} \cdot H_t\right)^2} \tag{33}$$

Intrinsic viscosity $[\mu]$ is defined by $[\mu](\dot{\gamma}) = \lim\limits_{H_t \to \infty} \frac{1}{H_t} \cdot \left(\frac{\mu(H_t, \dot{\gamma})}{\mu_p} - 1 \right)$ and in Quemada's model it is given by:

$$[\mu](\dot{\gamma}) = \frac{[\mu]_0 + [\mu]_\infty \cdot \sqrt{\frac{\dot{\gamma}}{\dot{\gamma}_c}}}{1 + \sqrt{\frac{\dot{\gamma}}{\dot{\gamma}_c}}} \tag{34}$$

Now, from the constitutive equation $\tau(t,y) = \mu(H_t(t,y), \dot{\gamma}(t,y)) \cdot \dot{\gamma}(t,y)$ of one of the rheological models described above, from formula (26) for the rheology independent shear stress, and from a suitable analytical formula for the shear strain rate, it is possible to derive a formula for the local hematocrit.

Let us consider this last topic. Axisymmetric flow velocity fields in small arteries and arterioles can de described by an empirical formula (Popel and Johnson 2005, Dillon, 2012):

$$u(t,y) = u_M \cdot (1 - y^q) \cdot f(t) \qquad 0 \le y \le 1 \tag{35}$$

Here $y = \frac{r}{R}$, $f(t)$ is a periodic function of time, u_M is the maximum velocity on the axis and $q \ge 2$ giving the degree of blunting of the profile. In this case the flow is pulsatile, not oscillatory, so $f(t)$ is always positive, with maximum equal to 1 and minimum greater than a lower bound of 0.3. It is phase-shifted relative to the cardiac cycle, depending of the position of the conduit in the arterial tree.

The pulsatile flow is: $Q(t) = 2\pi \cdot R^2 \cdot \int_0^1 y \cdot u(t,y) \cdot dy = \pi \cdot R^2 \cdot u_M \cdot \frac{q}{q+2} \cdot f(t)$ (36)

The shear velocity is given by: $\dot{\gamma}(t,y) = -\frac{1}{R} \frac{\partial}{\partial y} u(t,y) = q \cdot \frac{u_M}{R} \cdot y^{q-1} \cdot f(t)$ (37)

Formula (26) for the shear stress can be written: $\tau(t,y) \approx \frac{R \cdot \Delta P_M}{2 \cdot L} \cdot y \cdot f(t)$

So both, shear rate and shear stress are known in each point of the conduit. Substituting the known values of $\tau(t,y)$ and $\dot{\gamma}(t,y)$ in the apparent viscosity formula $\mu(H_t, \dot{\gamma}) = \frac{\tau}{\dot{\gamma}}$, an approximate formula that allows the determination of the hematocrit field is obtained:

$$\mu\left(H_t(t,y), q \cdot \frac{u_M}{R} \cdot y^{q-1} \cdot f(t) \right) \approx \frac{R^2 \cdot \Delta P_M}{2 \cdot L \cdot q \cdot u_M} \cdot y^{2-q} \tag{38}$$

Because the assumed shear velocity is independent of the axial coordinate z, a field $H_t(t, y)$ independent of z is derived from (38).

An alternative and more rigorous approach to the derivation of hematocrit field employs the migration potential (Phillips et al. 1992, Chen et al. 2003). In a quasi-steady state, after the suspension flow is well established, the migration potential Π must be constant. From equation (14), this is equivalent to the constancy of $H_t \cdot \dot{\gamma} \cdot \mu^{\lambda}(H_t, \dot{\gamma})$. However, $\dot{\gamma} = \frac{\tau}{\mu}$ and from equation (7): $\mu(H_t, \dot{\gamma}) = \frac{1}{\varphi(\tau, H_t)}$ So when there is equilibrium in the hydrodynamic diffusion process and the shear stress field is known:

$$H_t \cdot \tau \cdot \varphi^{1-\lambda}(H_t, \tau) = const. \tag{39}$$

As said above, in the case of oxygen, both fields near the wall, of shear rate and of hematocrit, could influence fluid to wall mass transport in the diffusive layer adjacent to the endothelium. In a first approximation, the flux density J_S of a certain substance through the diffusive boundary layer can be described by this formula (Tarbell and Qiu 2006):

$$J_S = k_{F-W} \cdot (C_B - C_E) \tag{40}$$

Here C_B is the concentration in the lumen just outside the diffusive boundary layer, C_E is the concentration in the surface of the endothelium, and k_{F-W} is a mass transfer coefficient. Assuming a well-mixed entrance flow and a developing diffusive boundary layer, the following proportionality relation can be approximately applied to estimate the mass transfer coefficient (Tarbell and Qiu 2006, Caro et al. 2012): $k_{F-W} \propto \sqrt[3]{\dot{\gamma}_w}$ Taking into account that $\dot{\gamma} = h(\tau, H_t)$, the permeability of the boundary layer verifies:

$$k_{F-W} \propto \sqrt[3]{h(\tau_w, H_{t,w})} \tag{41}$$

It is reasonable to expect an increase in the local viscosity when the local hematocrit increases. So, for a given shear stress in the wall τ_w (which is independent of the rheology and as consequence of the hematocrit and its distribution), the mass transfer coefficient should be a decreasing function of the local hematocrit near the wall. [3]

---

[3] In the case of oxygen, it is possible to guess that the concentration just outside the diffusive boundary layer can be considered as an increasing function $C_B(H_{t,w})$ of the wall hematocrit. The hematocrit field is rheology dependent, as will be seen below. Then it is possible to expect that oxygen concentration near the wall is also rheology dependent.

(C.2) A framework for a simplified numerical approach

Velocity profiles, pressures, local viscosity fields, shear rates and wall shear stresses are obtained by digital simulation, in straight segments of small arteries under pulsated flow conditions. Hematocrit fields are introduced in the viscosity of generalized Newtonian models to describe the effect of axial accumulation through viscosity fields in the equations of fluid dynamics.

Due to the symmetry of both the spatial domain and the flow, finite differences could have been used. However, finite elements (Ames 1992, Gershenfeld 1999) were applied, to ease the comparison with more realistic settings in which less symmetric spatial domains appear and spatially inhomogeneous discretization grids are more convenient.

Well known commercial software (COMSOL) already used by one of the present authors (Suárez-Bagnasco et al. 2013) was applied to the digital simulation of the equations. After a conversion to a weak form, the transport equations are solved using a version of a (Galerkin based) finite element discretization method. Possible spurious oscillations are controlled by numerical stabilization techniques available in the digital simulation code, without having to recourse to an impracticable (due to hardware limitations) dense mesh (COMSOL 2011).

The effects of the resultant hemodynamics on the parameters of fluid-to-wall mass transport processes are estimated from wall shear rates by means of approximate analytical formulae of diffusive boundary layer theory (Tarbell and Qiu 2006).

(D) Results

(D.1) Analytical results

Quasi-steady flow fields

From equation (21) and (22), introducing an arbitrary viscosity field $\mu(t,r)$ it follows:

$$\rho \cdot \frac{\partial u(t,r)}{\partial t} = \frac{\Delta P(t)}{L} + \frac{1}{r} \cdot \frac{\partial}{\partial r}\left(r \cdot \mu(t,r) \cdot \frac{\partial u}{\partial r}(t,r) \right) \tag{42}$$

Now, let us make a change of time and space scales and transform equation (42) to apply perturbation methods in the same spirit of the book by Lin and Segel (1988). Introduce the dimensionless radial distance $y = \frac{r}{R}$ relative to tube's radius R, the dimensionless time $\tau_P = \frac{t}{T_P}$ relative to the time scale T_P of the pulsatile pressure, a plasma viscosity diffusion time scale $T_{\nu p} = \frac{\rho_p \cdot R^2}{\mu_p} = \frac{R^2}{\nu_p}$ (being $\nu_p = \frac{\mu_p}{\rho_p}$ the kinematic viscosity of plasma) and the dimensionless parameter $\varepsilon = \frac{\rho}{\rho_p} \cdot \frac{T_{\nu p}}{T_P}$ Then (42) can be rewritten:

$$\varepsilon \cdot \frac{\partial u(\tau_P, y)}{\partial \tau_P} = \frac{R^2 \cdot \Delta P(\tau_P)}{\mu_p \cdot L} + \frac{1}{y} \cdot \frac{\partial}{\partial y}\left(y \cdot \frac{\mu(\tau_P, y)}{\mu_p} \cdot \frac{\partial u}{\partial y}(\tau_P, y) \right) \quad (43)$$

Here $\varepsilon = \frac{\rho}{\rho_p} \cdot \frac{R^2}{\nu_p} \cdot \frac{1}{T_P} = \frac{\rho}{\rho_p} \cdot \frac{R^2}{\nu_p} \cdot f_P$ being (by definition) $f_P = \frac{1}{T_P}$ the frequency of flow variation (heart frequency in Hz). Now introduce the Womersley number for plasma: $\alpha_p = R \cdot \sqrt{\frac{2\pi \cdot f_P}{\nu_p}}$ (44) It follows that: $\varepsilon = \frac{1}{2\pi} \cdot \frac{\rho}{\rho_p} \cdot \alpha_p^2$ (45)

For blood $\frac{\rho}{\rho_p} \approx 1.024$ and $\nu_p = 1.16 \times 10^{-6}\, m^2/s$ Then, for an arteriole with $R = 300\,\mu m$ the plasma viscosity diffusion time scale $T_{\nu p} = \frac{R^2}{\nu_p} \approx 7.76 \times 10^{-2}\, s$

If the dimensionless number ε is less than 0.1, the inertial term $\varepsilon \cdot \frac{\partial u(\tau_P, y)}{\partial \tau_P}$ may be neglected in a first approximation. For the abovementioned arteriole this happens when T_P is greater than 0.795 s (a frequency of the pressure wave less than 1.26 Hz).

Figure 1 shows the relation between frequency $f_P = \frac{1}{T_P}$ (in Hz) of the pressure wave and the arterial radius R (in m), for $\varepsilon = 0.1$:

$$\frac{1}{T_P} = 1.26 \cdot \left(\frac{0.0003}{R} \right)^2 \quad (46)$$

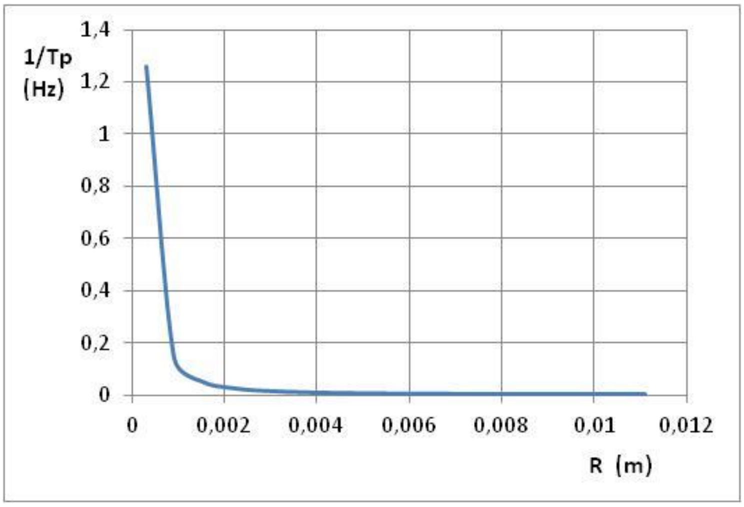

Figure 1 Estimation of an upper bound of pulse frequency (to be able to neglect inertial effects) as a function of the artery radius for radii between 300 µm and 1.1 cm.

Quasi-steady hematocrit fields

If particle migration is produced mainly orthogonally to the fluid velocity field, considering the assumed symmetry of the flow, in cylindrical coordinates, equation (15) simplifies to this one:

$$\frac{\partial H_t}{\partial t} = \frac{1}{r} \cdot \frac{\partial}{\partial r}\left(r \cdot D_{HD} \cdot \frac{\partial}{\partial r}\Pi \right) \tag{47}$$

Introducing a representative fluid velocity u_* (the velocity on the flow axis), tube's radius R, the global tube hematocrit $H_{t,g}$ and a measure of particle size a, a suitable order of magnitude estimation of the hydrodynamic diffusion coefficient $D_{HD} = K_c \cdot H_t^{\,2} \cdot a^2 \cdot \dot{\gamma}$ is:

$$D_{\otimes,*} \approx H_{t,g} \cdot a^2 \cdot \frac{u_*}{R} \tag{48}$$

Introduce the dimensionless radial distance $y = \frac{r}{R}$ relative to tube's radius and the dimensionless time $\tau_P = \frac{t}{T_P}$ relative to the time scale T_P of the pulsatile pressure. Define the hydrodynamic diffusion time scale $T_{HD} = \frac{R^2}{D_{\otimes,*}}$ and the dimensionless number:

$$\varepsilon = \frac{T_{HD}}{T_P} \approx \frac{R^3}{H_{t,g} \cdot a^2 \cdot u_*} \tag{49}$$

Then equation (43) can be re-written:

$$\varepsilon \cdot \frac{\partial H_t(\tau_P, y)}{\partial \tau_P} = \frac{1}{y} \cdot \frac{\partial}{\partial y}\left(y \cdot \frac{D_{HD}}{D_{\otimes,*}} \cdot \frac{\partial}{\partial y}\Pi(\tau_P, y) \right) \tag{50}$$

If ε is small enough, and if $\frac{\partial H_t(\tau_P, y)}{\partial \tau_P}$ remains suitably bounded in the time scale T_P, equation (45) can be approximated by its steady-state version:

$$\frac{1}{y} \cdot \frac{\partial}{\partial y}\left(y \cdot \frac{D_{HD}}{D_{\otimes,*}} \cdot \frac{\partial}{\partial y}\Pi(\tau_P, y) \right) \approx 0 \tag{51}$$

Then the function $y \cdot \frac{D_{HD}}{D_{\otimes,*}} \cdot \frac{\partial}{\partial y}\Pi(\tau_P, y)$ must be (practically) independent of the dimensionless radial distance. As it is reasonable to suppose that $\frac{\partial}{\partial y}\Pi(\tau_P, y)$ remains bounded when this radial distance approaches zero, it follows that $\frac{\partial}{\partial y}\Pi(\tau_P, y) \approx 0$. So in a quasi-steady state the migration potential must be (practically) independent of y.

Axial accumulation of formed elements and blood pumping power

Now let us estimate the pumping power, given in general by formula (29), for different rheological models (Newtonian, Power Law, Casson), considering axial accumulation. As already said, the flow in the conduit is restricted and the pressure head is adjusted to maintain a given flow. So, the first step in the procedure is to calculate flow according to formula (27). The second step is to derive the pressure gradient as a function of flow. The third and last step is to calculate the energy dissipation according to (29).

-Generalized Newtonian model

In this case $\dot{\gamma} = h_N\left(\tau, H_t\right) = \frac{1}{\mu_N\left(H_t\right)} \cdot \tau$ If $\mu_N\left(H_t(t,y)\right) = \mu_N(t,y)$, formula (27) gives:

$$Q(t) = \frac{\pi \cdot R^4 \cdot \Delta P(t)}{2 \cdot L} \cdot \int_0^1 y^3 \cdot \frac{1}{\mu_N\left(t,y\right)} \cdot dy \tag{52}$$

From formula (52) the pressure gradient across the vessel follows:

$$\frac{\Delta P}{L} = f(Q,R) = \frac{2 \cdot Q}{\pi \cdot R^4} \cdot \frac{1}{\left(\int_0^1 y^3 \cdot \frac{1}{\mu_N\left(t,y\right)} \cdot dy\right)} \tag{53}$$

Then, for the generalized Newtonian model the dissipated power is.

$$\dot{E} \approx \frac{2 \cdot L}{\pi \cdot R^4} \cdot \frac{1}{\left(\int_0^1 y^3 \cdot \frac{1}{\mu_N(t,y)} \cdot dy\right)} \cdot Q^2 \tag{54}$$

The dissipated power decreases when $F\left[\mu_N\right] = \int_0^1 y^3 \cdot \frac{1}{\mu_N(t,y)} \cdot dy$ increases. The functional $F\left[\mu_N\right]$ increases when the Newtonian viscosity field decreases towards the vessel's wall. The viscosity field $\mu_N\left(H_t\right)$ decreases when the hematocrit H_t decreases. So, in the framework of a generalized Newtonian model and equal other conditions (ceteris paribus), axial accumulation decreases energy dissipation and under isothermal conditions decreases entropy production.

-Power Law Model

For the Power Law model: $\dot{\gamma} = h_{PL}\left(\tau, H_t\right) = \left[\frac{1}{K_{PL}\left(H_t\right)} \cdot \tau\right]^{\frac{1}{n}}$ $0 < n < 1$

If $K_{PL}(H_t(t,y)) = K_{PL}(t,y)$ formula (27) gives:

$$Q(t) = \left(\pi \cdot R^{3+\frac{1}{n}} \cdot \int_0^1 y^{2+\frac{1}{n}} \cdot \frac{1}{[K_{PL}(t,y)]^{\frac{1}{n}}} \cdot dy \right) \cdot \left(\frac{\Delta P(t)}{2 \cdot L} \right)^{\frac{1}{n}} \tag{55}$$

Then:

$$\frac{\Delta P}{L} = f(Q,R) = \frac{2 \cdot Q^n}{\pi^n \cdot R^{3 \cdot n+1}} \cdot \frac{1}{\left(\int_0^1 y^{2+\frac{1}{n}} \cdot \frac{1}{[K_{PL}(t,y)]^{\frac{1}{n}}} \cdot dy \right)^n} \tag{56}$$

From (29) the dissipated power for a given flow is:

$$\dot{E}(t) \approx \frac{2 \cdot L}{\pi^n \cdot R^{3 \cdot n+1}} \cdot \frac{1}{\left(\int_0^1 y^{2+\frac{1}{n}} \cdot \frac{1}{[K_{PL}(t,y)]^{\frac{1}{n}}} \cdot dy \right)^n} \cdot Q^{n+1}(t) \tag{57}$$

The dissipated power decreases when $F[\mu_{PL}] = \int_0^1 y^{2+\frac{1}{n}} \cdot \frac{1}{[K_{PL}(t,y)]^{\frac{1}{n}}} \cdot dy$ increases. The functional $F[\mu_{PL}]$ increases when $K_{PL}(H_t)$ decreases towards the vessel's wall. But the field $K_{PL}(H_t)$ decreases when the hematocrit decreases. So, also in the framework of a Power Law model, and under equal other conditions, axial accumulation decreases energy dissipation and under isothermal conditions decreases entropy production.

-Casson model

In this case the shear rate vanishes when $0 \le \tau < \tau_y$, and when $\tau \ge \tau_y$ the shear rate is given by $\dot{\gamma} = h_C(\tau, H_t) = \frac{\left(\sqrt{\tau} - \sqrt{\tau_y(H_t)}\right)^2}{\mu_N(H_t)}$. The viscosity field ($\mu_N(H_t(t,y)) = \mu_N(t,y)$) that appears in the denominator is an asymptotic, hematocrit dependent Newtonian viscosity. The yield shear stress is assumed to be given by the empirical formula (Merrill 1969, Quemada 1978 (b)) where $2 \le p \le 3$ and $H_{t,*} \cong 0.1$ [4] :

$$\tau_y(H_t) = \tau_y(t,y) \approx c \cdot (H_t - H_{t,*})^{\,p} \tag{58}$$

---

[4] Under in vivo conditions always $H_t > H_{t,*}$

Equation (27) gives the flow: $Q(t) = \pi \cdot R^3 \cdot \left(\int_0^1 y^2 \cdot \frac{\left(\sqrt{\tau(t,y)} - \sqrt{\tau_y(t,y)}\right)^2}{\mu_N(t,y)} \cdot dy \right)$ (59)

Introduce the auxiliary variable: $x = \sqrt{\frac{R \cdot \Delta P(t)}{2 \cdot L}}$ (60)

From (59) and (60) it follows:

$$\frac{Q(t)}{\pi \cdot R^3} = \left(\int_0^1 \frac{y^3}{\mu_N(t,y)} \cdot dy \right) \cdot x^2 - 2 \cdot \left(\int_0^1 \frac{y^{\frac{5}{2}} \cdot \sqrt{\tau_y(t,y)}}{\mu_N(t,y)} \cdot dy \right) \cdot x + \left(\int_0^1 y^2 \cdot \frac{\tau_y(t,y)}{\mu_N(t,y)} \cdot dy \right) \quad (61)$$

Now, define a functional of the Newtonian asymptotic viscosity and the yield stress fields:

$$b\left[\mu_N, \tau_y\right] = \frac{\left(\int_0^1 \frac{y^{\frac{5}{2}} \cdot \sqrt{\tau_y(t,y)}}{\mu_N(t,y)} \cdot dy \right)}{\left(\int_0^1 \frac{y^3}{\mu_N(t,y)} \cdot dy \right)} \quad (62)$$

Then, define a functional of the Newtonian asymptotic viscosity and the yield stress fields that is also a function of the blood flow and vessel's radius[5]:

$$c\left[\mu_N, \tau_y; (Q,R)\right] = \frac{\left(\frac{Q(t)}{\pi \cdot R^3} - \int_0^1 y^2 \cdot \frac{\tau_y(t,y)}{\mu_N(t,y)} \cdot dy \right)}{\int_0^1 \frac{y^3}{\mu_N(t,y)} \cdot dy} \quad (63)$$

The solution with physical meaning of equation (61) can be written thus:

$$x = b + \sqrt{b^2 + c} \quad (64)$$

Taking into account (60), the pressure gradient to maintain a given flow is:

$$\frac{\Delta P}{L} = f(Q,R) = \frac{2}{R} \cdot \left(b + \sqrt{b^2 + c}\right)^2 \quad (65)$$

---

[5] From of equation (61) and the behavior of the integrands there it follows $\frac{Q(t)}{\pi \cdot R^3} > \int_0^1 y^2 \cdot \frac{\tau_y(t,y)}{\mu_N(t,y)} \cdot dy$: the functional defined by equation (63) takes always positive values.

Then the dissipated power for the Casson model in a quasi-steady state is:

$$\dot{E} \approx Q \cdot \Delta P = \frac{2 \cdot L}{R} \cdot \left(b + \sqrt{b^2 + c} \right) \cdot Q \tag{66}$$

If the hematocrit H_t decreases when the dimensionless radial distance increases, both the asymptotic viscosity $\mu_N(H_t)$ and the yield stress $\tau_y(H_t)$ (formula (58)) decrease from the vessel axis towards the vessel wall. Then the function $\frac{y^3}{\mu_N(t,y)}$ increases towards the wall. However, both $\frac{y^{\frac{5}{2}} \cdot \sqrt{\tau_y(t,y)}}{\mu_N(t,y)} = \frac{y^3}{\mu_N(t,y)} \cdot \sqrt{\frac{\tau_y(t,y)}{y}}$ and $y^2 \cdot \frac{\tau_y(t,y)}{\mu_N(t,y)} = \frac{y^3}{\mu_N(t,y)} \cdot \frac{\tau_y(t,y)}{y}$ can't increase as fast as $\frac{y^3}{\mu_N(t,y)}$ when the radial distance increases, or even they can decrease or vanish. As consequence the functional $b + \sqrt{b^2 + c}$ decreases if the hematocrit decreases from the vessel axis towards the wall: then, formula (66) shows that also in the framework of Casson model energy dissipation should decreases with axial accumulation.

Hematocrit fields from q-adic velocity profiles: a derivation of model m

The following mathematical formula for a spatially variable hematocrit (model m) was proposed for axisymmetric velocity patterns in straight segments of small arteries under quasi-stationary conditions, as a function of the dimensionless radial distance $y = \frac{r}{R}$ (Suárez-Ántola, 1980):

$$\frac{H_t(y)}{H_{t,M}} = 1 - \left(1 - \frac{H_{t,w}}{H_{t,M}} \right) \cdot y^m \tag{67}$$

From the tube global hematocrit $H_{t,g} = \frac{2 \cdot \pi \cdot \int_0^R r \cdot H_t(r) \cdot dr}{\pi \cdot R^2} = 2 \cdot \int_0^1 y \cdot H_t(y) \cdot dy$ a formula for the parameter m is derived:

$$m = 2 \cdot \frac{\left(H_{t,g} - H_{t,w} \right)}{\left(H_{t,M} - H_{t,g} \right)} \tag{68}$$

If m is known, wall hematocrit can be estimated:

$$H_{t,w} = H_{t,g} - \frac{m}{2} \cdot \left(H_{t,M} - H_{t,g} \right) \tag{69}$$

Figure 2 shows the parameter m as a function of the tube global hematocrit [6] for the case $H_{t,w} = 0$ and $H_{t,M} = 1$.

---

[6] The *discharge hematocrit* is obtained collecting a volume of blood circulating through a vein in a suitable recipient. If the velocity profile $u(r)$ is steady and axisymmetric, and if Q is the volumetric flow in the vein, the discharge hematocrit is: $H_{t,g}(disch.) = \frac{2 \cdot \pi \cdot \int_0^R r \cdot u(r) \cdot H_t(r) \cdot dr}{Q}$

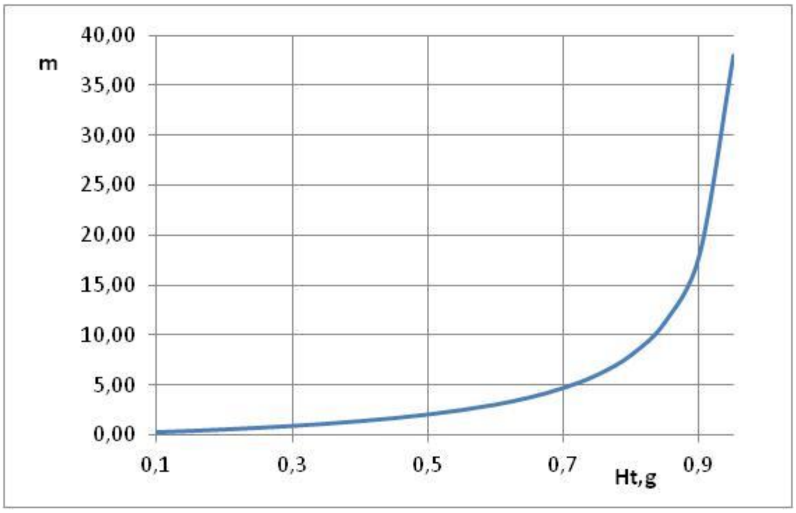

Figure 2: Relation between *m* and global hematocrit (for $H_{t,g}$ ranging from 10 to 95%)

Figure 3 shows the function $H_t(y)$ with $y = \frac{r}{R}$ for five values of the global tube hematocrit for the particular case $H_{t,w} = 0$ and $H_{t,M} = 1$.

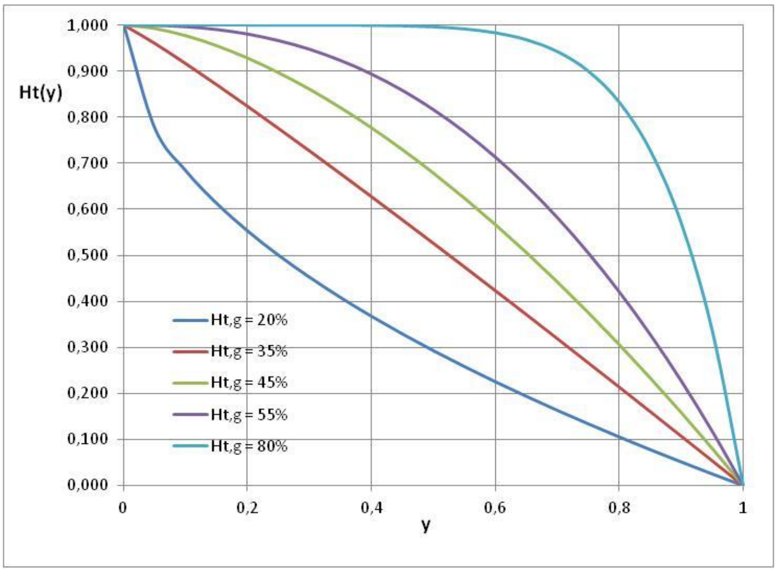

Figure 3: Local hematocrit as a function of distance from vessel axis for different global hematocrits $H_{t,g}$.

The *tube hematocrit* can be measured stopping the flow and emptying the vessel blood contain in a suitable recipient and can be calculated by the formula: $H_{t,g}(tube) = \frac{2 \cdot \pi \cdot \int_0^R r \cdot H_t(r) \cdot dr}{\pi \cdot R^2}$ (Baskurt et al. 2007; Nichols et al. 2011; Chandran et al. 2012)

Now, let us explore the possibility of deriving this model m from known quasi-steady velocity profiles.

For quasi-steady axisymmetric flow velocity fields that can de described by the empirical formula (35) ($u(t,y) = u_M \cdot (1 - y^q) \cdot f(t)$), the hematocrit can be obtained from equation (38) because in this case both shear rates field $\dot{\gamma}(t,y) = q \cdot \frac{u_M}{R} \cdot y^{q-1} \cdot f(t)$ and shear stresses field $\tau(t,y) = \frac{R \cdot \Delta P_M}{2 \cdot L} \cdot y \cdot f(t)$ are known.

The rheology independent field of shear stresses can be related with the pulsatile wall shear stress $\tau_w(t)$ by:

$$\tau(t,y) \approx \frac{R \cdot \Delta P_M}{2 \cdot L} \cdot y \cdot f(t) = \tau_w(t) \cdot y \tag{70}$$

The rheology dependent field of shear rates can be related with the pulsatile wall shear rate $\dot{\gamma}_w(t)$ by:

$$\dot{\gamma}(t,y) \approx q \cdot \frac{u_M}{R} \cdot y^{q-1} \cdot f(t) = \dot{\gamma}_w(t) \cdot y^{q-1} \tag{71}$$

To continue, it is necessary to specify a formula for $\mu(H_t, \dot{\gamma})$, that is a rheological model, in formula (38). Let us introduce the viscosity of blood adjacent to the vessel wall:

$$\mu_w = \frac{\tau_w}{\dot{\gamma}_w} = \frac{R^2 \cdot \Delta P_M}{2 \cdot q \cdot L \cdot u_M} \tag{72}$$

Taking into account (70), (71) and (72), formula (38) can be rewritten thus:

$$\mu\left(H_t(t,y), \dot{\gamma}_w(t) \cdot y^{q-1}\right) \approx \mu_w \cdot y^{2-q} \tag{73}$$

Quasi-steady hematocrit field when the apparent viscosity is given by the generalized Newtonian model

If the viscosity is given by formula (31) ($\mu_N(H_t) \approx \frac{\mu_p}{\left(1 - \frac{H_t}{H_{t,M}}\right)^k}$), from (73) it follows model m formula for the local hematocrit:

$$H_t(y) \approx H_{t,M} \cdot \left(1 - \left(1 - \frac{H_{t,w}}{H_{t,M}}\right) \cdot y^m\right) \tag{74}$$

$$m = \frac{q-2}{k} \qquad (q \geq 2) \tag{75}$$

$$\left(1 - \frac{H_{t,w}}{H_{t,M}}\right) = \left(\frac{\mu_p}{\mu_w}\right)^{\frac{1}{k}} \tag{76}$$

From (74) and the formula that relates the local with the tube hematocrit $H_{t,g} = 2 \cdot \int_0^1 y \cdot H_t(y) \cdot dy$, the wall hematocrit $H_{t,w} = H_t(1)$ results as function of maximum packing hematocrit $H_{t,M}$, the global (tube) hematocrit, and the parameter m (determined in terms of the assumed known parameters q and k from (75)):

$$H_{t,w} = H_{t,g} - \frac{m}{2}\cdot\left(H_{t,M} - H_{t,g}\right) \tag{77}$$

From (77): $1-\dfrac{H_{t,w}}{H_{t,M}} = \left(1-\dfrac{H_{t,g}}{H_{t,M}}\right)\cdot\left(1+\dfrac{m}{2}\right)$ From (75): $1+\dfrac{m}{2} = 1+\dfrac{q-2}{2\cdot k}$ ($q \geq 2$)

From the formula that relates the viscosity with the hematocrit in a generalized Newtonian model $\mu_N\left(H_{t,w}\right) = \mu_w \approx \dfrac{\mu_p}{\left(1-\dfrac{H_{t,w}}{H_{t,M}}\right)^k}$ and $\mu_N\left(H_{t,g}\right) = \mu_{N,g} \approx \dfrac{\mu_p}{\left(1-\dfrac{H_{t,g}}{H_{t,M}}\right)^k}$

Then, from these last four equations we obtain a formula that gives μ_w as function of the parameters μ_p, k and $H_{t,M}$ of the relation between the viscosity and the hematocrit, the blunting parameter q of blood flow profile and (through $\mu_{N,g}$) the global hematocrit $H_{t,g}$:

$$\mu_w \approx \left(\frac{1}{1+\dfrac{(q-2)}{2\cdot k}}\right)^k \cdot \mu_{N,g} \tag{78}$$

Quasi-steady hematocrit field when the apparent viscosity is given by Quemada´s model

If the viscosity is given by formulae (33) and (34), $\mu_Q\left(H_t,\dot\gamma\right) = \dfrac{\mu_p}{\left(1-\dfrac{[\mu](\dot\gamma)}{k}\cdot H_t\right)^k}$ and $[\mu](\dot\gamma) = \dfrac{[\mu]_0 + [\mu]_\infty\cdot\sqrt{\dfrac{\dot\gamma}{\dot\gamma_c}}}{1+\sqrt{\dfrac{\dot\gamma}{\dot\gamma_c}}}$, from equations (73) and (71) the following formula for the local hematocrit is obtained:

$$H_t(t,y) \approx \frac{k\cdot\left(1+\sqrt{\dfrac{\dot\gamma_w(t)}{\dot\gamma_c}\cdot y^{q-1}}\right)}{\left([\mu]_0 + [\mu]_\infty\cdot\sqrt{\dfrac{\dot\gamma_w(t)}{\dot\gamma_c}\cdot y^{q-1}}\right)}\cdot\left(1-\left(\frac{\mu_p}{\mu_w}\right)^{\frac{1}{k}}\cdot y^m\right) \tag{79}$$

The parameter m is also given by formula (75) as in the generalized Newtonian model. However, instead of a constant maximum packing fraction $H_{t,M}$, a field $H_{t,M}(t,y)$ of local maximum packing fractions results:

$$H_{t,M}(t,y) = \frac{k\cdot\left(1+\sqrt{\dfrac{\dot\gamma_w(t)}{\dot\gamma_c}\cdot y^{q-1}}\right)}{\left([\mu]_0 + [\mu]_\infty\cdot\sqrt{\dfrac{\dot\gamma_w(t)}{\dot\gamma_c}\cdot y^{q-1}}\right)} \tag{80}$$

When the maximum of the dimensionless shear rate $\frac{\dot{\gamma}_w(t)}{\dot{\gamma}_c}$ is small enough, or when its minimum is big enough, formula (80) gives a constant maximum packing fraction, $\frac{k}{[\mu]_0}$ and $\frac{k}{[\mu]_\infty}$ respectively.

Asymptotic steady hematocrit field when the apparent viscosity is given by Casson´s model.

Let us consider strictly steady conditions and describe blood rheology with Casson model. When the shear stress $\tau_w \cdot y$ at the dimensionless radial distance y is greater than the yield stress τ_y, the shear velocity there is different from zero. The yield stress is a local value that increases when the local hematocrit increases according to equation (58). Here we suppose that $H_t(y) > H_{t,*}$ for every dimensionless radial distance. When there is axial accumulation $\tau_y(H_t) = \tau_y(y)$ decreases from a maximum value $\tau_y(H_{t,M})$ in the vessel axis towards a minimum value at the wall $\tau_y(H_{t,w})$. Local shear stress $\tau(y) = \tau_w \cdot y$ increases from zero in vessel axis towards τ_w at the vessel wall. If $\tau_w > \tau_y(H_{t,w})$, the decreasing function $\tau_y(y)$ and the increasing function $\tau(y)$ have one intersection point y_c given by the unique solution of the equation $\tau(y) = \tau_y(y)$. As we don´t know yet the field $H_t(y)$ we can't specify y_c, but we know that there is one, and we know that when $y_c < y$, then $\dot{\gamma} > 0$. In this case equation (73) gives:

$$\mu_C\left(H_t, \dot{\gamma}_w \cdot y^{q-1}\right) = \left(\sqrt{\frac{\tau_y(H_t)}{\dot{\gamma}_w \cdot y^{q-1}}} + \sqrt{\mu_N(H_t)}\right)^2 = \mu_w \cdot y^{2-q} \qquad (81)$$

However, if $y \le y_c$ then $\dot{\gamma} = 0$ (we have piston flow in the inner cylinder $0 \le y \le y_c$).

Taking into account that $\sqrt{\mu_N(H_t)} = \frac{\sqrt{\mu_p}}{\left(1 - \frac{H_t}{H_{t,M}}\right)^{\frac{k}{2}}}$, equation (81) can be recast as follows:

$$\sqrt{\frac{\tau_y(H_t)}{\tau_w}} \cdot \frac{1}{y^{\frac{1}{2}}} + \frac{\sqrt{\frac{\mu_p}{\mu_w}} \cdot y^{\frac{q-2}{2}}}{\left(1 - \frac{H_t}{H_{t,M}}\right)^{\frac{k}{2}}} = 1 \qquad y \ge y_c \qquad (82)$$

Now, let us define $\varepsilon = \sqrt{\frac{\tau_y(H_{t,M})}{\tau_w}}$ so (82) can be written thus:

$$\varepsilon \cdot \sqrt{\frac{\tau_y(H_t)}{\tau_y(H_{t,M})}} \cdot \frac{1}{y^{\frac{1}{2}}} + \frac{\sqrt{\frac{\mu_p}{\mu_w}} \cdot y^{\frac{q-2}{2}}}{\left(1 - \frac{H_t}{H_{t,M}}\right)^{\frac{k}{2}}} = 1 \qquad (84)$$

When the dimensionless parameter $\varepsilon = \sqrt{\dfrac{\tau_y\left(H_{t,M}\right)}{\tau_w}}$ is small enough, a perturbation analysis gives the following successive approximations:

Zero order ($\varepsilon = 0$):
$$H_{t,0}(y) \approx H_{t,M} \cdot \left(1 - \left(\frac{\mu_p}{\mu_w}\right)^{\frac{1}{k}} \cdot y^m\right) \qquad (85)$$

Here $m = \dfrac{q-2}{k}$ and $\dfrac{\mu_p}{\mu_w} = \left(1 - \dfrac{H_{t,w}}{H_{t,M}}\right)^k$ So, under steady conditions model m formula is obtained as the zero-order approximation.

First order ($\varepsilon = \sqrt{\dfrac{\tau_y\left(H_{t,M}\right)}{\tau_w}}$ is retained in equation (84) and $\tau_y\left(H_{t,0}\right)$ is substituted in place of $\tau_y\left(H_t\right)$):

$$\sqrt{\frac{\tau_y\left(H_{t,0}(y)\right)}{\tau_w(t)}} \cdot \frac{1}{y^{\frac{1}{2}}} + \frac{\sqrt{\dfrac{\mu_p}{\mu_w}} \cdot y^{\frac{q-2}{2}}}{\left(1 - \dfrac{H_{t,1}(y)}{H_{t,M}}\right)^{\frac{k}{2}}} \approx 1$$

From this approximate equation a first order approximation $H_{t,1}(y)$ to the steady hematocrit field is obtained:

$$\frac{H_{t,1}(y)}{H_{t,M}} \approx 1 - \left(\frac{\mu_p}{\mu_w}\right)^{\frac{1}{k}} \cdot y^m \cdot \frac{1}{\left(1 - \varepsilon \cdot \sqrt{\dfrac{\tau_y\left(H_{t,0}(y)\right)}{\tau_y\left(H_{t,M}\right)}} \cdot \dfrac{1}{y^{\frac{1}{2}}}\right)}$$

Now, make the further approximation:

$$\frac{1}{\left(1 - \varepsilon \cdot \sqrt{\dfrac{\tau_y\left(H_{t,0}(y)\right)}{\tau_y\left(H_{t,M}\right)}} \cdot \dfrac{1}{y^{\frac{1}{2}}}\right)} \approx 1 + \varepsilon \cdot \sqrt{\frac{\tau_y\left(H_{t,0}(y)\right)}{\tau_y\left(H_{t,M}\right)}} \cdot \frac{1}{y^{\frac{1}{2}}}$$

Then this formula for the hematocrit field is finally derived:

$$H_{t,1}(y) \approx H_{t,M} \cdot \left(1 - \left(\frac{\mu_p}{\mu_w}\right)^{\frac{1}{k}} \cdot y^m - \left(\frac{\mu_p}{\mu_w}\right)^{\frac{1}{k}} \cdot \varepsilon \cdot \sqrt{\frac{\tau_y\left(H_{t,0}(y)\right)}{\tau_y\left(H_{t,M}\right)}} \cdot y^{m-\frac{1}{2}}\right) \qquad (86)$$

When $m = \dfrac{q-2}{k} > \dfrac{1}{2}$ or equivalently when $q > 2 + \dfrac{k}{2}$, the decreasing function of y given by formula (86) is well behaved in the whole interval of radial distances.

Hematocrit fields from the migration potential and from Scott's micro-rheological model

Hematocrit from migration potential

When there is equilibrium in the hydrodynamic diffusion process and the shear stress field is known, equation (39) gives the corresponding condition of equal migration potential everywhere in terms of the function $\frac{\dot{\gamma}}{\tau} = \varphi(\tau, H_t) = \frac{1}{\mu(H_t, \dot{\gamma})}$ introduced in equation (7). From (39) and (70) the following formula is obtained for the hematocrit field under quasi-steady conditions:

$$y = \frac{H_{t,w}(t)}{H_t(t,y)} \cdot \left(\frac{\varphi(H_t(t,y), \tau_w \cdot y \cdot f(t))}{\varphi(H_{t,w}(t), \tau_w \cdot f(t))} \right)^{\lambda-1} \qquad (87)$$

The parameter λ is greater than 1 and known. The relation between tube and local hematocrit ($H_{t,g} = 2 \cdot \int_0^1 y \cdot H_t(t,y) \cdot dy \le H_{t,M}$) allows the derivation of the wall hematocrit for a slow enough pulsatile flow. Wall shear stress τ_w is known and rheology independent. The positive function $f(t)$ is assumed known. The size of the suspended particles doesn't appear in equation (87). So, in principle, the quasi-steady hematocrit field predicted by the hydrodynamic diffusion theory is independent of particle´s size.

-For a generalized Newtonian model $\varphi_N(\tau, H_t) = \frac{1}{\mu_p} \cdot \left(1 - \frac{H_t}{H_{t,M}}\right)^k$. In this case (87) gives:

$$y = \frac{H_{t,w}}{H_t(y)} \cdot \left(\frac{1 - \frac{H_t(y)}{H_{t,M}}}{1 - \frac{H_{t,w}}{H_{t,M}}} \right)^{(\lambda-1)\cdot k} \qquad (88)$$

-Let us consider now the following modified Quemada's model:

$$\varphi_Q(\tau, H_t) = \frac{1}{\mu_p} \cdot \left(1 - \frac{H_t}{H_{t,M}(\tau)}\right)^k \qquad (89)$$

Here, by definition:

$$H_{t,M}(\tau) = \frac{k \cdot \left(1 + \sqrt{\frac{\tau}{\tau_c}}\right)}{\left([\mu]_0 + [\mu]_\infty \cdot \sqrt{\frac{\tau}{\tau_c}}\right)} \qquad (90)$$

In (90) τ_c is a constant critical shear stress and $\tau = \tau(t,y) = \tau_w \cdot y \cdot f(t)$

Then, from (87) and (89):
$$y=\frac{H_{t,w}(t)}{H_t(t,y)}\cdot\left(\frac{1-\dfrac{H_t(t,y)}{H_{t,M}(\tau_w\cdot y\cdot f(t))}}{1-\dfrac{H_{t,w}(t)}{H_{t,M}(\tau_w\cdot f(t))}}\right)^{(\lambda-1)\cdot k} \tag{91}$$

-For Casson model, whenever $\frac{\tau_y(H_t)}{\tau}\leq 1$, $\varphi_C(\tau,H_t)=\frac{1}{\mu_N(H_t)}\cdot\left(1-\sqrt{\frac{\tau_y(H_t)}{\tau}}\right)^2$ and $\varphi_C(\tau,H_t)$ is zero if $\frac{\tau_y(H_t)}{\tau}>1$. From (87) and $\tau_y(H_t(t,y))\leq\tau_w\cdot y\cdot f(t)$, it follows:

$$y=\frac{H_{t,w}}{H_t}\cdot\left(\frac{1-\dfrac{H_t}{H_{t,M}}}{1-\dfrac{H_{t,w}}{H_{t,M}}}\right)^{(\lambda-1)\cdot k}\cdot\left(\frac{1-\sqrt{\dfrac{\tau_y(H_t)}{\tau_w\cdot y\cdot f(t)}}}{1-\sqrt{\dfrac{\tau_y(H_t)}{\tau_w}}}\right)^{(\lambda-1)\cdot 2} \tag{92}$$

Under strictly steady conditions, we have seen above (in the discussion immediately before equation (81)) that $\tau_y(H_t(y))=\tau_w\cdot y$ has only one solution, the critical radial distance y_c, such that there is piston flow in the inner cylinder $0\leq y\leq y_c$ and in the annular region outside it:
$$y=\frac{H_{t,w}}{H_t(y)}\cdot\left(\frac{1-\dfrac{H_t}{H_{t,M}}}{1-\dfrac{H_{t,w}}{H_{t,M}}}\right)^{(\lambda-1)\cdot k}\cdot\left(\frac{1-\sqrt{\dfrac{\tau_y(H_t)}{\tau_w\cdot y}}}{1-\sqrt{\dfrac{\tau_y(H_t)}{\tau_w}}}\right)^{(\lambda-1)\cdot 2} \tag{93}$$

For blood k is always very near 2. As first approximation it is possible to take $\lambda\approx\frac{3}{2}$, so if $k=2$ then $(\lambda-1)\cdot k\approx 1$. This allows the derivation of explicit analytical formulae for the hematocrit field. For the generalized Newtonian model and the modified Quemada's model the problem reduces to an algebraic equation. For Casson model, if $\varepsilon=\sqrt{\frac{\tau_y(H_{t,M})}{\tau_w}}$ is small, it is possible to obtain analytical formulae by a method of successive approximations, like the one already applied for the derivation of an asymptotic steady hematocrit field, in the framework of Casson´s model and q-adic velocity profiles. The corresponding calculation for a constant migration potential will not be done here.

-If $(\lambda-1)\cdot k\approx 1$, from (88), for the generalized Newtonian model the hematocrit field is given by the following formula, already given in Phillips et al. 1992:
$$H_t(y)=\frac{H_{t,M}}{1+\left(\dfrac{H_{t,M}}{H_{t,w}}-1\right)\cdot y} \tag{94}$$

The wall hematocrit $H_{t,w}$ is determined from (94) and the tube hematocrit formula

$$H_{t,g} = 2 \cdot \int_0^1 y \cdot H_t(y) \cdot dy \tag{95}$$

The following implicit equation is obtained:

$$H_{t,g} = \frac{2 \cdot H_{t,M}}{\left(\dfrac{H_{t,M}}{H_{t,w}} - 1\right)} \cdot \left\{ 1 - \frac{1}{\left(\dfrac{H_{t,M}}{H_{t,w}} - 1\right)} \cdot \log_e\left(\frac{H_{t,M}}{H_{t,w}}\right) \right\} \tag{96}$$

If $(\lambda - 1) \cdot k \approx 1$, for the modified Quemada´s model, from (90) and (91), the field of hematocrit is:

$$H_t(t, y) = \frac{H_{t,M}(\tau)}{1 + \left(\dfrac{H_{t,M}(\tau)}{H_{t,w}(t)} - 1\right) \cdot y} \tag{97}$$

Here $H_{t,M}(\tau)$ is given by equation (90) and the shear stress is $\tau = \tau(t, y) = \tau_w \cdot y \cdot f(t)$. The wall hematocrit $H_{t,w}(t)$ is determined from (96) and the tube hematocrit formula giving another implicit equation if the global tube hematocrit is assumed known.

Hematocrit from Scott's model

Under quasi-steady conditions and with an axisymmetric flow pattern, radial diffusion and radial migration flux densities will be equal and opposite: $H_t \cdot u_m = \dfrac{D}{R} \cdot \dfrac{\partial}{\partial y} H_t$ (98)

In general, both particles migration velocity u_m and diffusion coefficient D will be functions of the radial distance. Here we assume axial migration, so $u_m = -|u_m|$.

Let us introduce a local dimensionless Péclet number: $$Pe(y) = \frac{R \cdot |u_m|(y)}{D(y)} \tag{99}$$

Taking into account that $H_t(y)$ must be always less than the maximum packing fraction $H_{t,M}$, to integrate (98) under steady conditions from a dimensionless radial distance y up to the wall, two cases should be considered:

If $H_{t,w} \cdot \exp\left[\int_0^1 Pe(\zeta) \cdot d\zeta\right] \le H_{t,M}$ the hematocrit field is given by the formula, valid for every $0 \le y \le 1$:

$$H_t(y) = H_{t,w} \cdot \exp\left[\int_y^1 Pe(\zeta) \cdot d\zeta\right] \tag{100}$$

If $H_{t,w} \cdot \exp\left[\int_0^1 Pe(\zeta) \cdot d\zeta\right] > H_{t,M}$, let us introduce the critical radial distance y_c such that:

$$H_{t,w} \cdot \exp\left[\int_{y_c}^1 Pe(\zeta) \cdot d\zeta\right] = H_{t,M} \tag{101}$$

Then $H_t(y) = H_{t,w} \cdot \exp\left[\int_y^1 Pe(\zeta) \cdot d\zeta\right]$ in the interval $y_c \le y \le 1$ (102 a)

In the interval $0 \le y \le y_c$, $H_t(y) = H_{t,M}$ (102 b)

In any case, the local hematocrit field $H_t(y)$ is related with the tube hematocrit by the (often quoted) formula:

$$H_{t,g} = 2 \cdot \int_0^1 y \cdot H_t(y) \cdot dy \le H_{t,M} \tag{103}$$

To simplify let us assume $u_m(y) = -u_w \cdot y$ and $D = D_0$ constant. Introduce the dimensionless wall Péclet number:

$$Pe_w = Pe(1) = \frac{R \cdot u_w}{D_0} \tag{104}$$

Then the steady hematocrit field is given, from (100) and (104), by the formula:

$$H_t(y) = H_{t,w} \cdot \exp\left[\frac{Pe}{2} \cdot \left(1 - y^2\right)\right] = H_t(0) \cdot \exp\left[-\frac{Pe}{2} \cdot y^2\right] \tag{105}$$

Then, from (103) it follows $H_t(0) = \dfrac{H_{t,g} \cdot Pe}{2 \cdot \left(1 - \exp\left[-\frac{Pe}{2}\right]\right)}$ and from this last equation and from (105):

$$H_t(y) = \frac{H_{t,g} \cdot Pe_w}{2 \cdot \left(1 - \exp\left[-\frac{Pe_w}{2}\right]\right)} \cdot \exp\left[-\frac{Pe_w}{2} \cdot y^2\right] \tag{106}$$

If the maximum packing fraction is attained at a positive critical radial distance y_c, this parameter verifies the equation (derived from (101)):

$$H_{t,w} \cdot \exp\left[\frac{Pe_w}{2} \cdot \left(1 - {y_c}^2\right)\right] = H_{t,M} \tag{107}$$

Then:

$$H_t(y) = H_{t,w} \cdot \exp\left[\frac{Pe_w}{2} \cdot \left(1 - y^2\right)\right] \qquad y_c \le y \le 1 \tag{108 a}$$

$$H_t(y) = H_{t,M} \qquad 0 \le y \le y_c \tag{108 b}$$

The wall Péclet number $Pe_w = \dfrac{u_w}{\left(\frac{D_0}{R}\right)} = \dfrac{u_w \cdot H_{t,g}}{\left(\frac{D_0}{R} \cdot H_{t,g}\right)}$ gives a measure of the magnitude of the migration flux relative to the diffusive flux: in principle Pe could increase from near zero, for a uniform distribution of cells in a cross section of the vessel (corresponding to a diffusion-dominated regime) towards values an order of magnitude greater than 1 for an hematocrit highly concentrated in the neighborhood of the vessel axis (corresponding to a full migration-dominated regime).

Scott obtained an approximate analytical formula for the migration velocity which relates said velocity with particle size (through a particle radius a), vessel radius R, a measure of suspending fluid viscosity (through plasma viscosity μ_p), a measure of cell's rigidity (through a surface tension α), a measure of the maximum flow velocity V_M and the dimensionless radial distance: $u_m \approx -\dfrac{11}{70} \cdot \dfrac{\mu_p \cdot {V_M}^2}{\alpha} \cdot \left(\dfrac{a}{R}\right)^3 \cdot \left(\dfrac{r}{R}\right)$ (Scott 2005). Then the migration velocity adjacent to the vessel wall is:

$$u_w \approx \frac{11}{70} \cdot \frac{\mu_p \cdot {V_M}^2}{\alpha} \cdot \left(\frac{a}{R}\right)^3 \tag{109}$$

As consequence, wall Péclet number increases when the particle diameter increases. So, to the extent that this approach can be applied to a suspension of particles with different sizes, the smaller particles will be mode uniformly distributed relative to the larger ones: in the flowing blood case, platelets will accumulate less towards the axis than red blood cells. This is a significant difference with the prediction of the hydrodynamic diffusion theory. According to this last theory steady concentration profiles should be independent of particle sizes.

(D.2) Numerical results

A Navier-Stokes equation (incompressible fluid) with a steady viscosity field $\mu(H_t(\vec{r}))$ (a particular case of equation (10) with a generalized Newtonian model) was solved numerically for two rigid cylinders, one segment of an arteriole of radius $R = 0.3\,mm$ and length $L = 6\,mm$ and the other, a segment of an artery with $R = 6\,mm$ and $L = 40\,mm$. A fluid density $1050\, {kg}/{m^3}$ was used in all the numerical calculations.

Due to the symmetry restrictions, numerical solution reduces to the digital simulation of fluid flow according to the equation (42) for a steady viscosity field:

$$\rho \cdot \frac{\partial u(t,r)}{\partial t} = \frac{\Delta P(t)}{L} + \frac{1}{r} \cdot \frac{\partial}{\partial r}\left(r \cdot \mu(H_t(r)) \cdot \frac{\partial u}{\partial r}(t,r) \right) \qquad (110)$$

Boundary conditions: $u(t,R) = 0$, $P_{output}(t) = 0$, $P_{input}(t)$ Several input pulse shapes $P_{input}(t)$ were introduced, both pulsatile and oscillatory. Two pulsatile pressures: a wave shape $P_E(t)$ (Figure 4) obtained experimentally in a hemodynamic work bench (Suárez-Bagnasco et al. 2013) and the sum $P_P(t)$ (Figure 5) of an average pressure with a harmonic oscillating pressure. Two oscillatory pressures: harmonic oscillations of approximately 1 Hz and 10 Hz, $P_1(t)$ (Figure 6) and $P_{10}(t)$ (Figure 7) respectively.

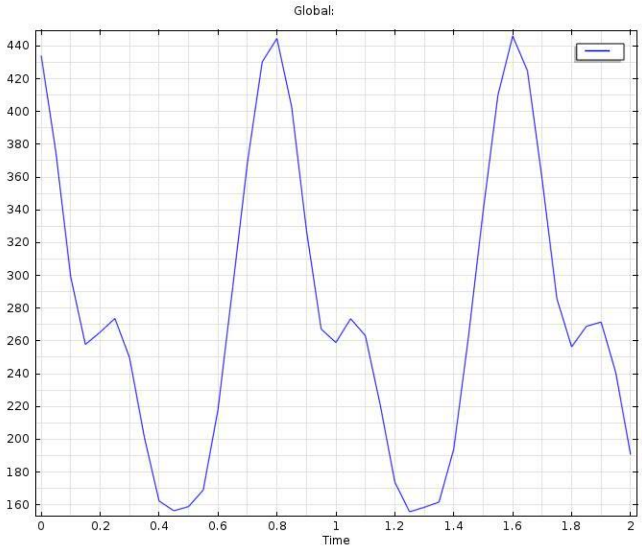

Figure 4: Experimental pattern of pulsatile pressure, with systolic value 440 Pa and diastolic value 160 Pa, obtained in vitro in a work bench.

Analytical formula used to calculate $P_E(t)$:

4*(68.47+29.85*cos(t[1/s]*7.666)+1.167*sin(t[1/s]*7.666)+5.808*cos(2*t[1/s]*7.666)-11.41*sin(2*t[1/s]*7.666)+4.27*cos(3*t[1/s]*7.666)-2.542*sin(3*t[1/s]*7.666)+0.2223*cos(4*t[1/s]*7.666)+1.579*sin(4*t[1/s]*7.666)+0.2855*cos(5*t[1/s]*7.666)-0.2226*sin(5*t[1/s]*7.666)-0.3875*cos(6*t[1/s]*7.666)-0.0622*sin(6*t[1/s]*7.666))

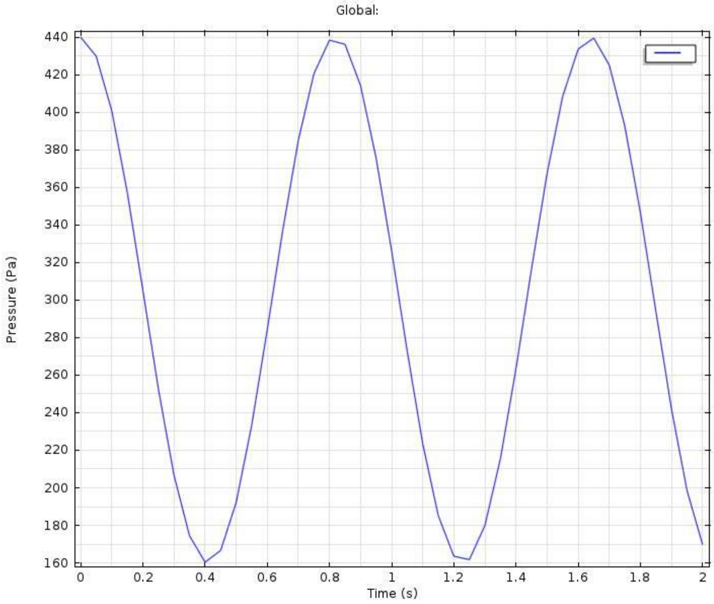

Figure 5: Pulsatile pressure with systolic value 440 Pa, diastolic value 161 Pa, mean value 300 Pa and 1 Hz (approximate) frequency.

Analytical formula used to calculate $P_P(t)$:

140*cos(t[1/s]*7.666)+300

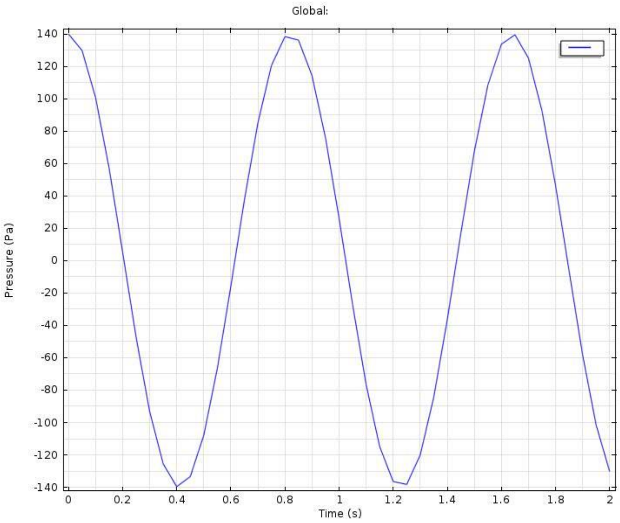

Figure 6: Oscillatory pressure of (approximate) frequency 1 Hz, with systolic value 140 Pa and diastolic value -140 Pa.

Analytical formula used to calculate $P_1(t)$:

140*cos(t[1/s]*7.666)

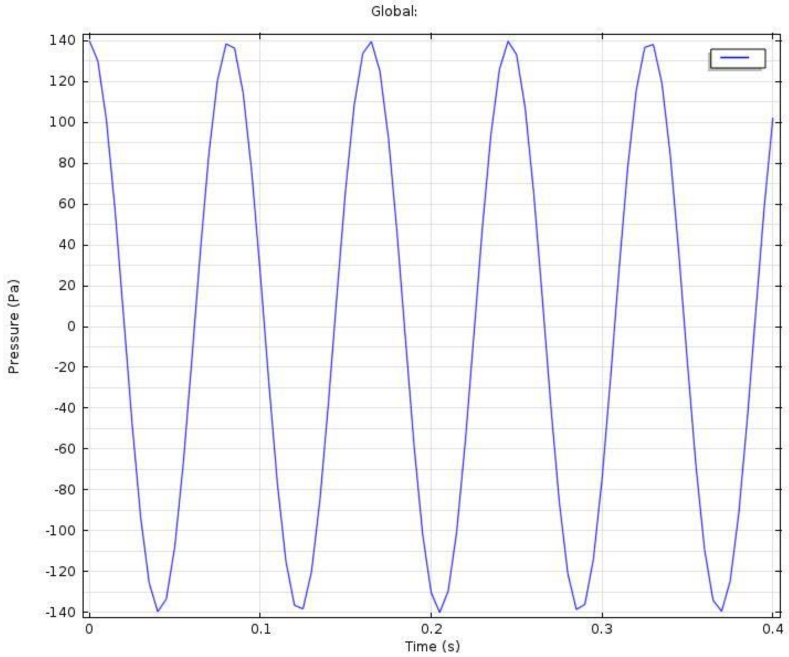

Figure 7: Oscillatory pressure of (approximate) frequency 10 Hz, with systolic value 140 Pa and diastolic value -140 Pa.

Analytical formula used to calculate $P_1(t)$:

(140*cos(t[1/s]*76.66))

Figure 8 shows one finite element mesh generated by the digital simulation code.

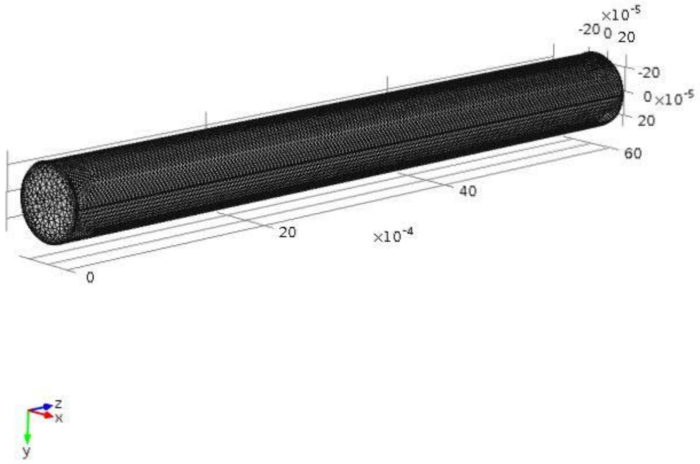

Figure 8: A finite element mesh for the arteriole.

A time interval comprised between 0 a 2s was used for digital simulation purposes, with increments of 0.05s.

Two cases of the generalized Newtonian model were implemented, both with $H_{t,M} = 1$ and $\mu_p = 0.0012\ Pa \cdot s$.

Case 1:
$$\mu_N(H_t) = \frac{\mu_p}{(1 - \beta \cdot H_t)} \tag{111}$$

Case 1 equation for the relation between viscosity and hematocrit was not considered previously in the present work. Here $\beta = 0.2$ is selected for digital simulation purposes. In Case 1 a simplified model m was employed: model $m(s)$ that follows from equations (67) and (68), putting $H_{t,w} = 0$ and $H_{t,M} = 1$:

$$H_t(y) = \left(1 - y^{m(s)}\right) \qquad m(s) = 2 \cdot \frac{H_{t,g}}{1 - H_{t,g}}$$

Three values of the global hematocrit $H_{t,g}$ were used: 35 %, 45 % and 55 %. The corresponding values of $m(s)$ are 1.08, 1.64 and 2.44 respectively.
As consequence of the chosen relations between viscosity and hematocrit, and between hematocrit and radial distance, the implemented viscosity field is:

$$\mu_{N,m(s)}(y) = \frac{\mu_p}{\left(1 - \beta \cdot \left(1 - y^{m(s)}\right)\right)} \tag{112}$$

Analytical formula used as input by the software to calculate the viscosity field given by equation (112):

0.0012[Pa*s]/(1-0.2*(1-(sqrt(x*x+y*y)/Rtube)^m))

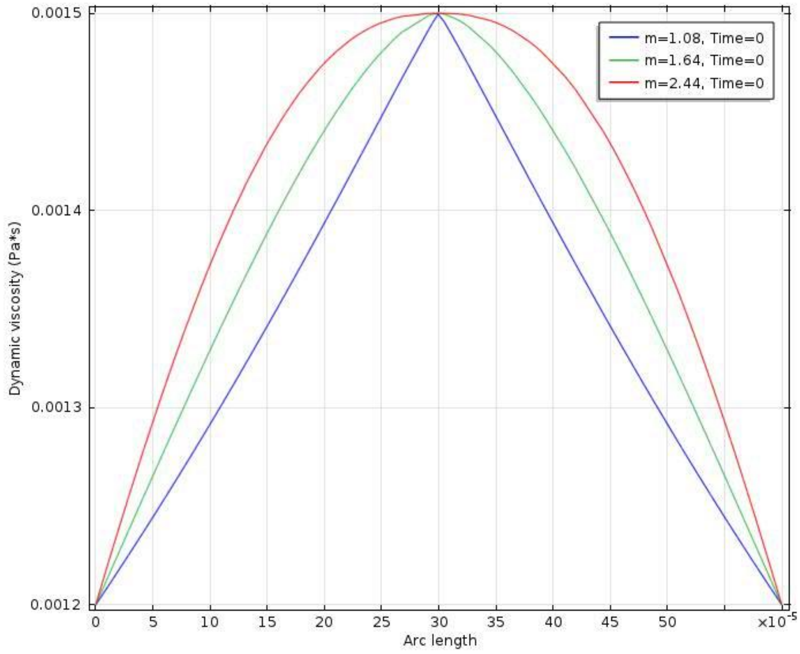

Figure 9: Viscosity fields along an arteriole diameter for different values of $m(s)$

Case 2: $$\mu_N\left(H_t\right)=\frac{\mu_p}{\left(1-H_t\right)^2} \tag{113}$$

Case 2 equation is obtained from equation (31) with $H_{t,M} = 1$ and $k = 2$. Equation (106) for the hematocrit field was implemented in this case. As consequence of the new chosen relations between viscosity and hematocrit, and between hematocrit and radial distance, the following viscosity field was implemented:

$$\mu_{N,S}\left(y\right)=\frac{\mu_p}{\left(1-\frac{H_{t,g}\cdot Pe_w}{2\cdot\left(1-\exp\left[-\frac{Pe_w}{2}\right]\right)}\cdot\exp\left[-\frac{Pe_w}{2}\cdot y^2\right]\right)^2} \tag{114}$$

Three values of the wall Péclet number were used: 0.2, 1.0 and 2.0 with a global hematocrit $H_{t,g}$ of 45 %.

Analytical formula used as input by the software to calculate the viscosity field given by equation (114):

0.0012[Pa*s]/(1-(A/(1-exp(-A)))*0.45*exp(-A*(sqrt(x*x+y*y)/Rtube)^2))^2 A= (Pe$_w$) /2

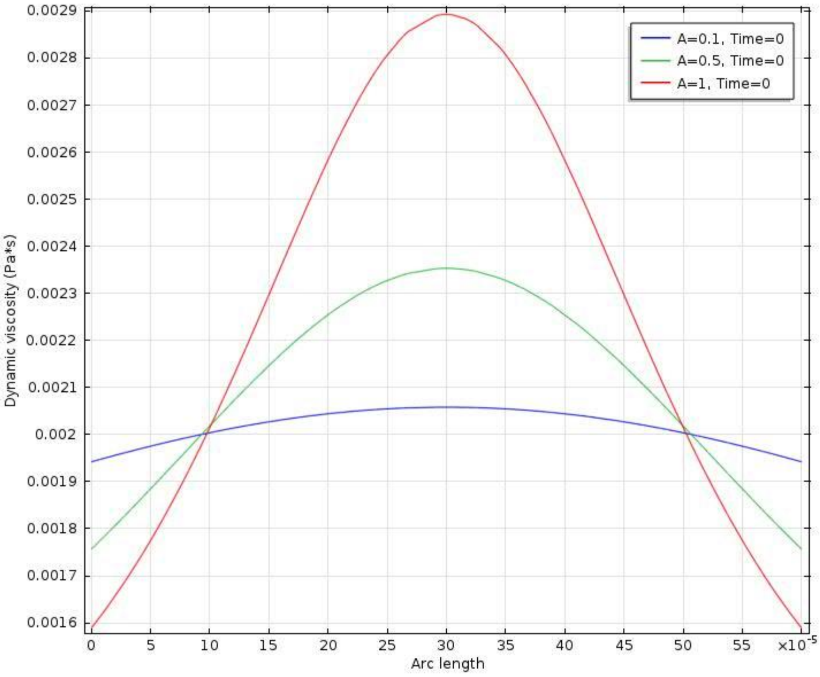

Figure 10: Viscosity fields along an arteriole diameter for different values of $A=\frac{Pe_w}{2}$

A whole blood viscosity of $0.0035\ Pa\cdot s$ was employed in numerical calculations of blood flow in absence of axial accumulation, for comparison purposes.

(D 2.1) Velocity profiles and shear rates for an arteriole

Input pressure $P_E(t)$, viscosity fields according to Figure 9.

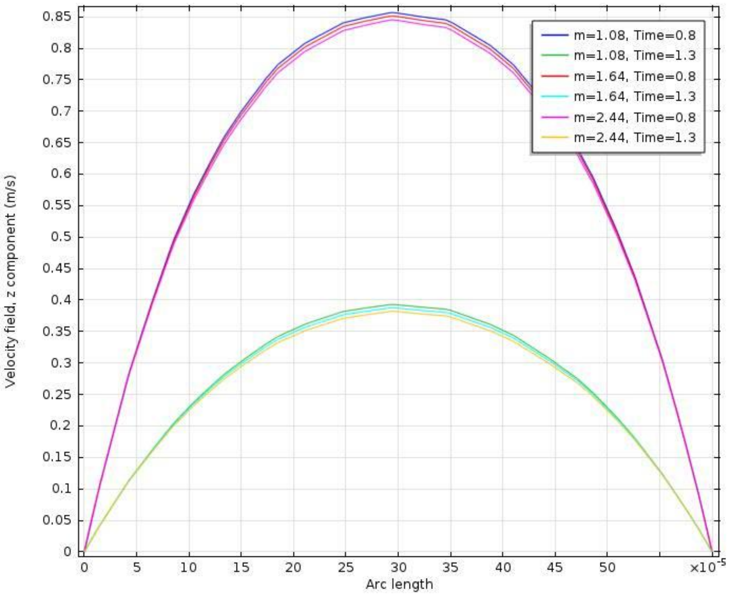

Figure 11: Velocity fields along an arteriole diameter for the experimentally determined pressure input different values of $m(s)$ for systole and diastole.

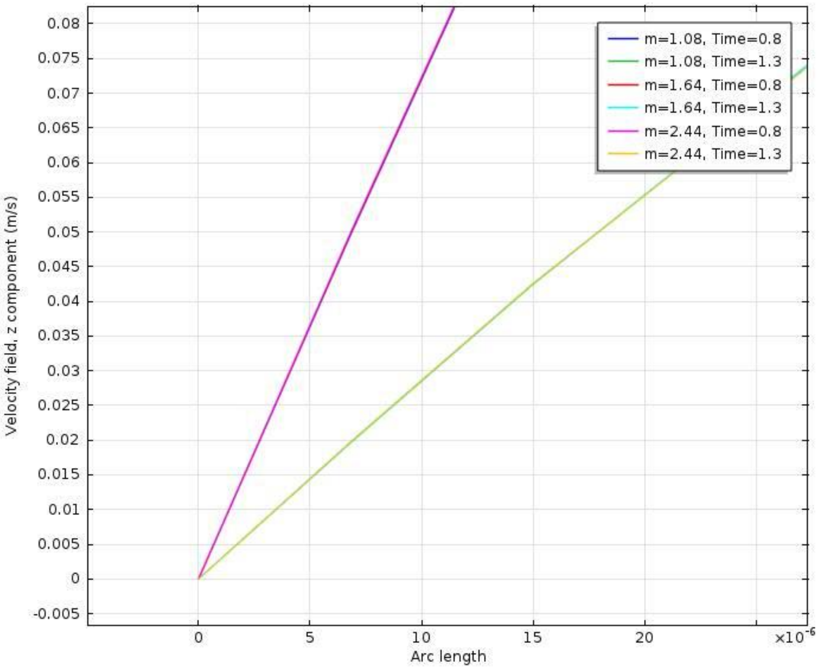

Figure 12: Details of velocity fields near the arteriole wall for systole and diastole.

Input pressure $P_1(t)$, viscosity fields according to Figure 9.

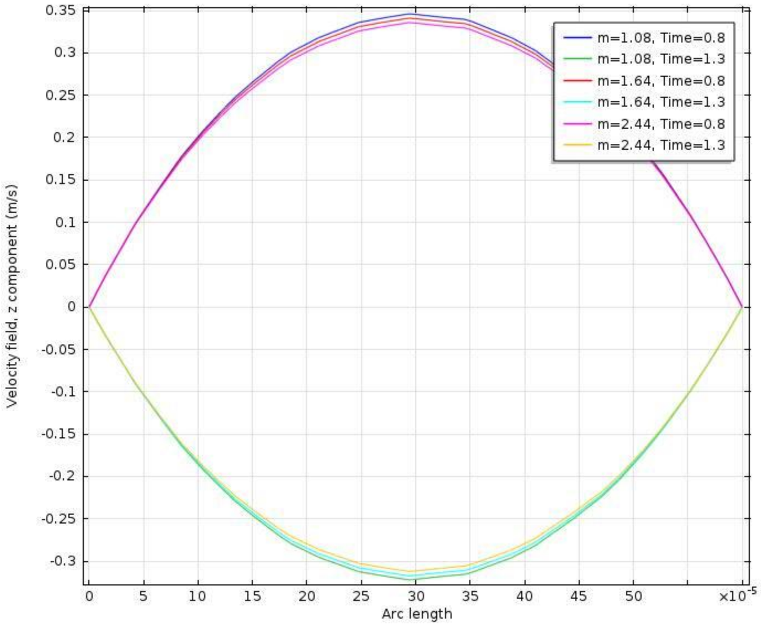

Figure 13: Velocity fields along an arteriole diameter for different values of $m(s)$ and different instants for the considered oscillatory input for systole and diastole.

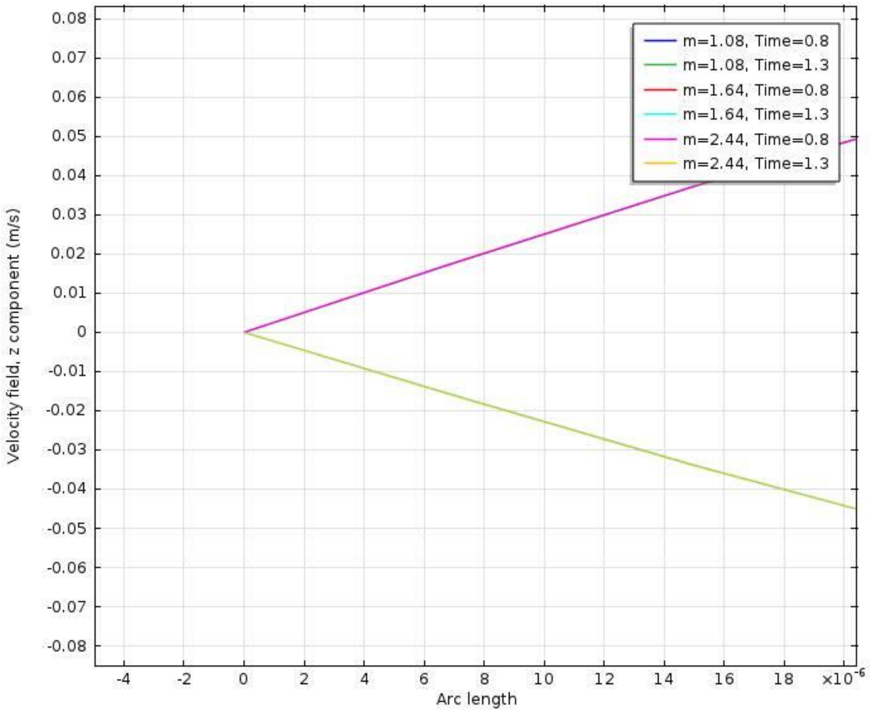

Figure 14: Details of velocity fields near the arteriole wall for systole and diastole.

Input pressure $P_{10}(t)$, viscosity fields according to Figure 9.

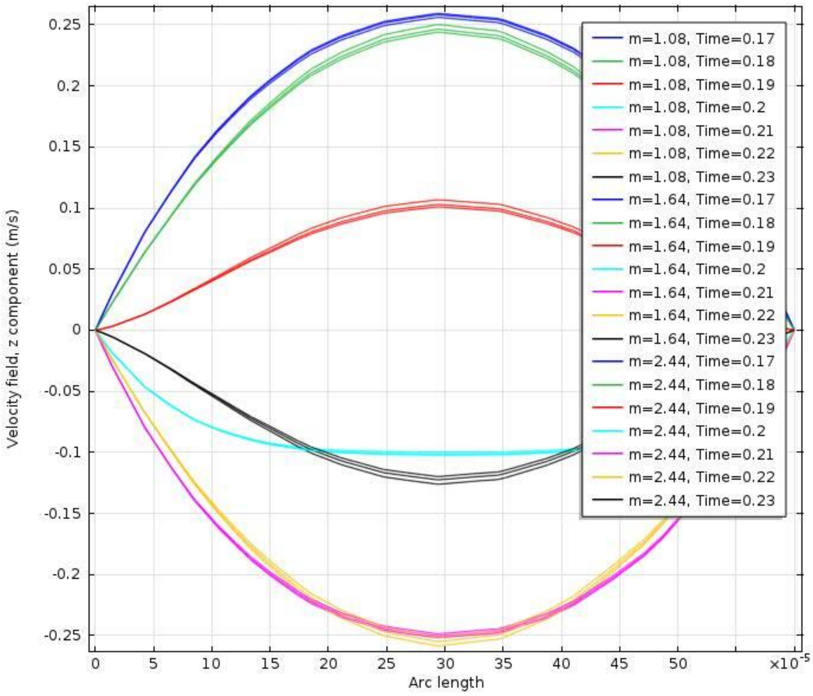

Figure 15: Velocity fields along an arteriole diameter for different values of $m(s)$ and different instants for the considered oscillatory input for different instants.

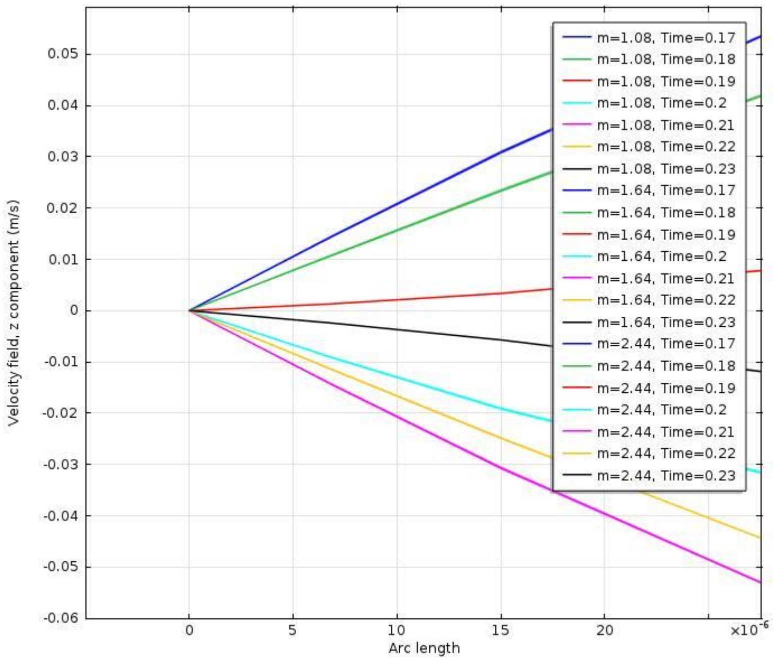

Figure 16: Details of velocity fields near the arteriole wall

Input pressure $P_P(t)$, viscosity fields according to Figure 10.

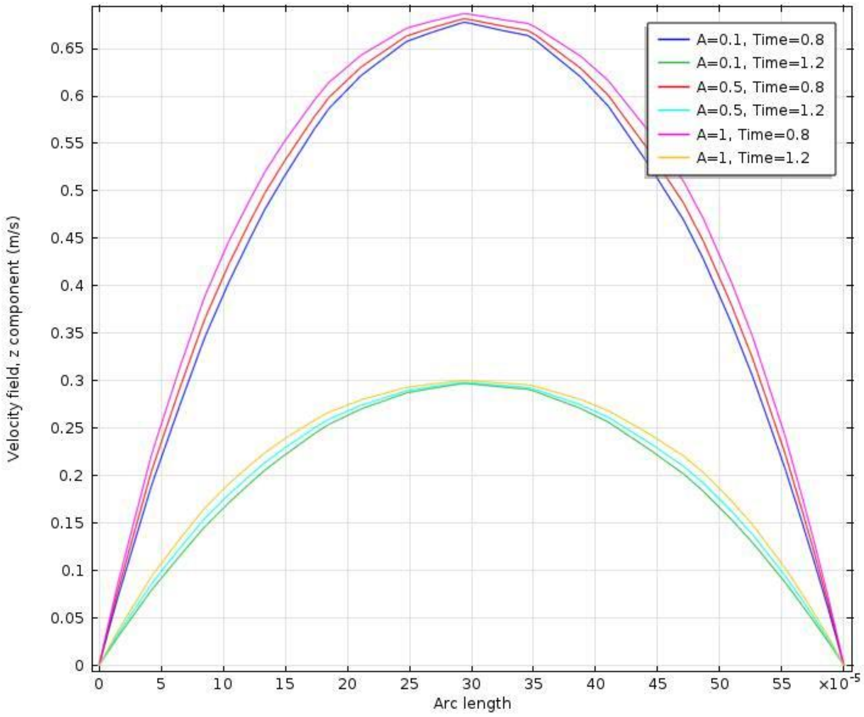

Figure 17: Velocity fields along an arteriole diameter for different values of $A = \frac{Pe_w}{2}$ and different instants for the considered oscillatory input for systole and diastole.

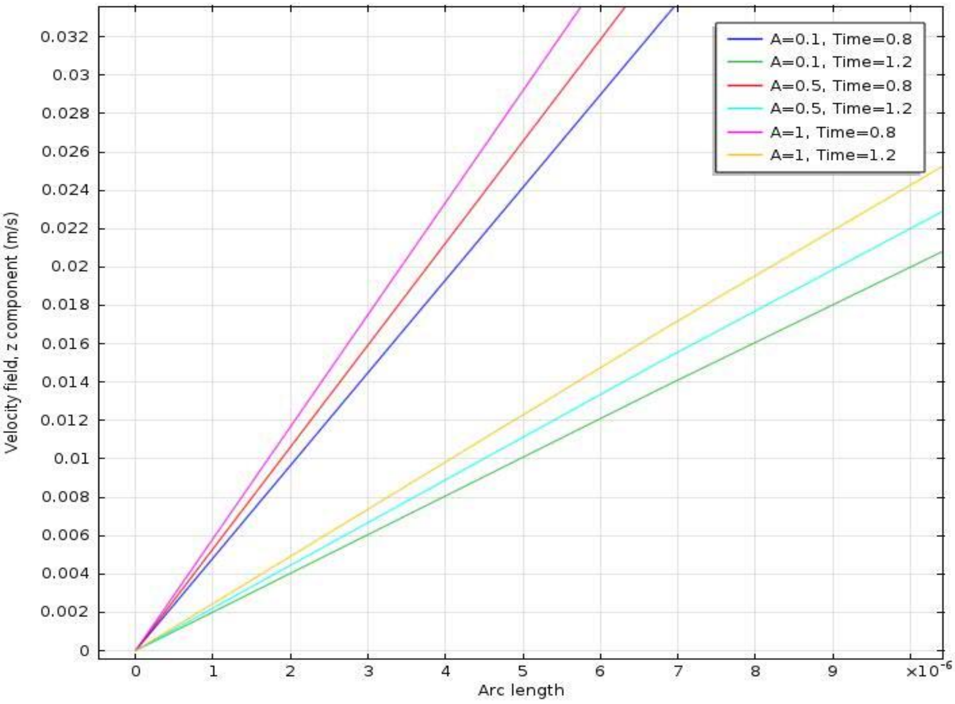

Figure 18: Details of velocity fields near the arteriole wall for systole and diastole.

Input pressure $P_1(t)$, viscosity fields according to Figure 10.

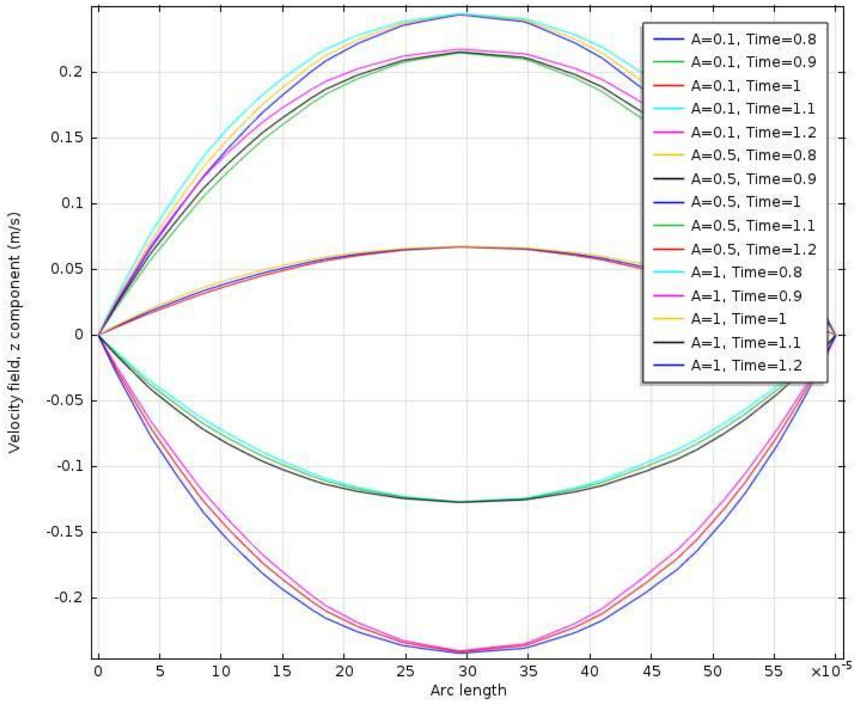

Figure 19: Velocity fields along an arteriole diameter for different values of $A = \frac{Pe_w}{2}$ and different instants for the considered oscillatory input for different instants

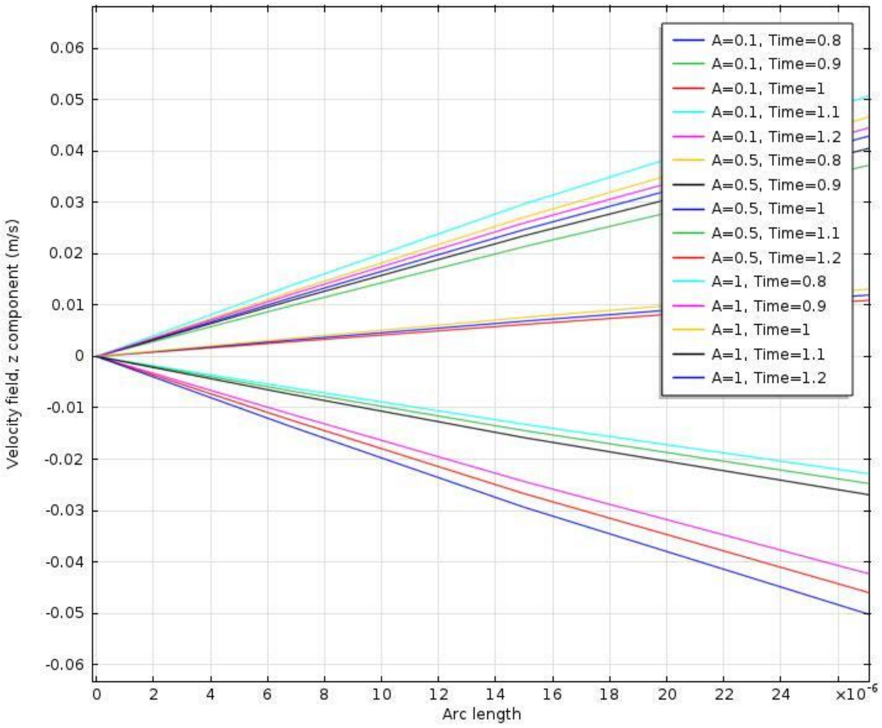

Figure 20: Details of velocity fields near the arteriole wall

Input pressure $P_{10}(t)$, viscosity fields according to Figure 10.

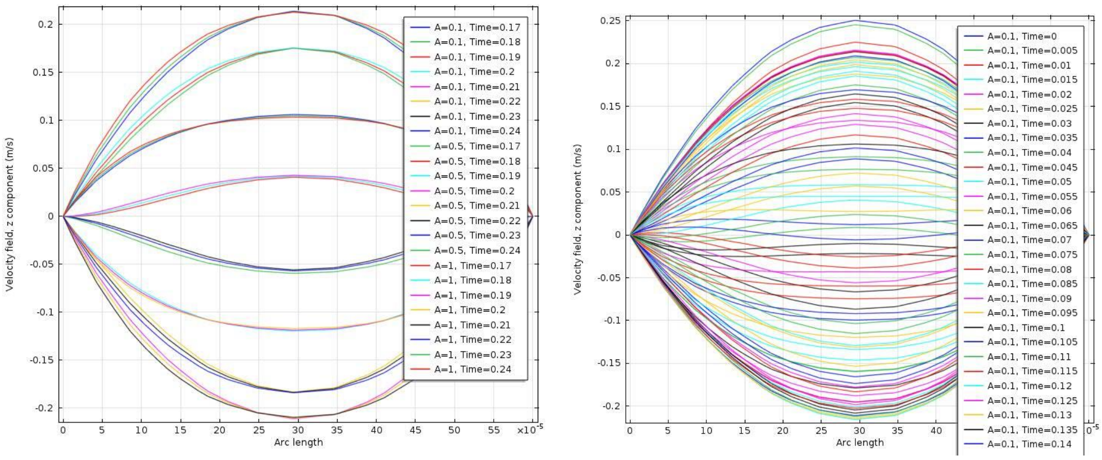

Figure 21: Velocity fields along an arteriole diameter for different values of $A = \frac{Pe_w}{2}$ and different instants for the considered oscillatory input for different instants.

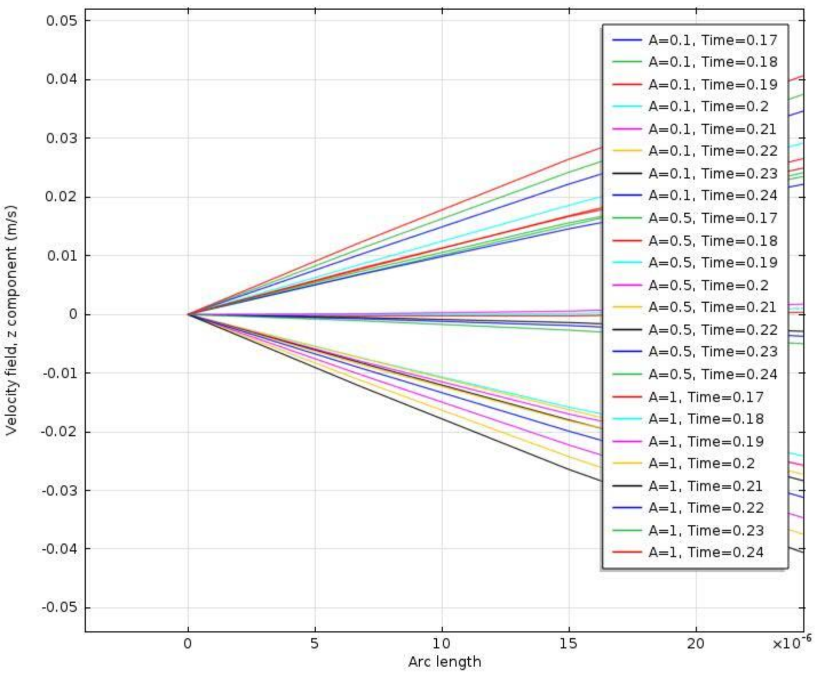

Figure 22: Details of velocity fields near the arteriole wall

(D 2.2) Velocity profiles and shear rates for an artery

Input pressure $P_1(t)$, viscosity fields according to Figure 10.

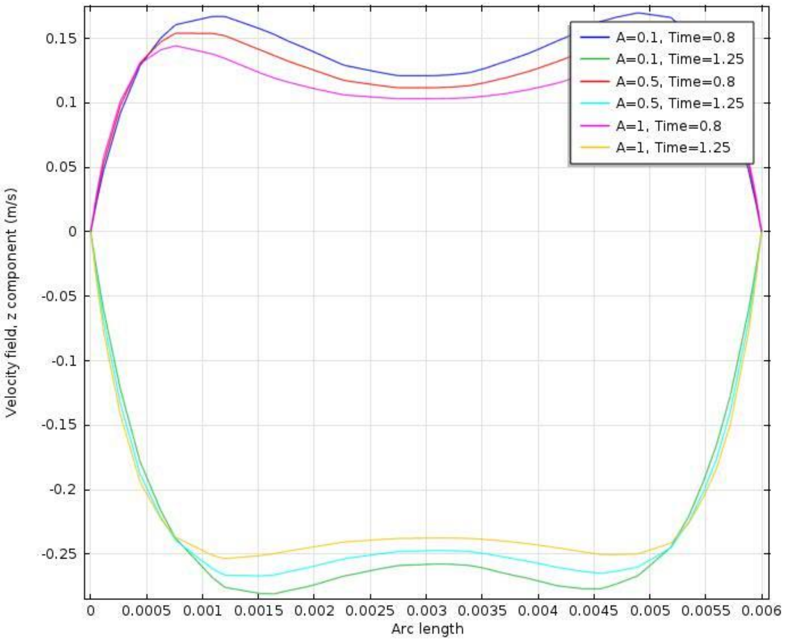

Figure 23: Velocity fields along an artery diameter for different values of $A = \frac{Pe_w}{2}$ and different instants for the considered oscillatory input for systole and diastole.

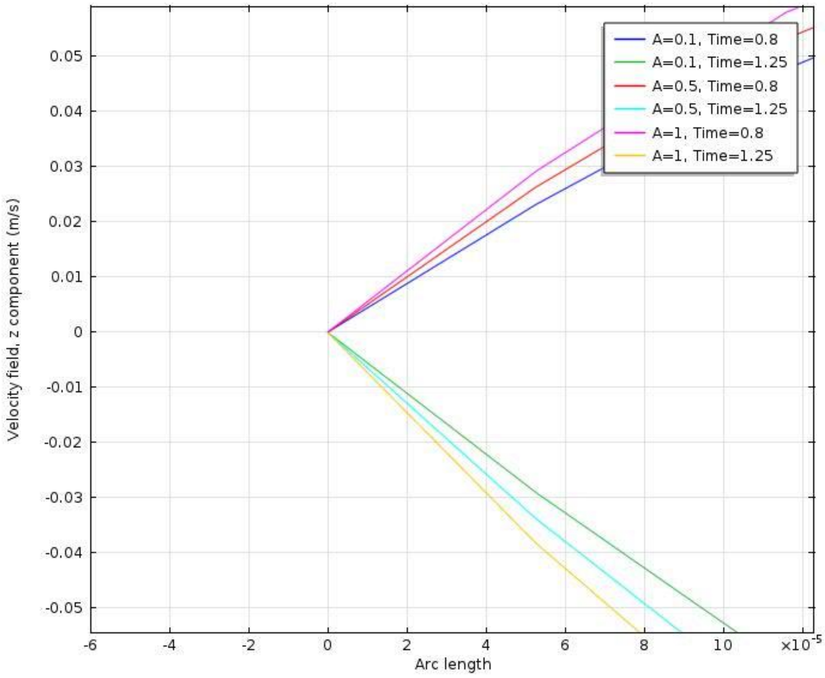

Figure 22: Details of velocity fields near the artery wall for systole and diastole.

(E) Discussion and Conclusions

-CFD results show that for an arteriole the quasi-steady solution of fluid dynamics equation, with axial accumulation, agrees with the numerical solution when the pulse frequency is of the order of 1 Hz or less. For frequencies of 10 Hz or more inertial effects can´t be neglected and the quasi-steady solution is not applicable.

-CFD results show that for an artery the quasi-steady solution of fluid dynamics equation, with axial accumulation, doesn´t agree with the numerical solution, even when the pulse frequency is of the order of 1 Hz. In Figures 15 and 21, notice the change in the sign of the curvature of the velocity profiles for time instants in a neighborhood of the times in which the input pressures cross by zero. In these instants the time derivative of the pressure pulse takes its maximum values, and the accelerations are different at different distances from the vessel axis. Blood adjacent to the wall, up to the inflection point of the velocity profile, accelerate positively or negatively more than the blood in the region adjacent to the flow axis.

-According to CFD calculations, in the arteriole, when quasi-steady conditions apply, systolic and diastolic velocity profiles are the same for the experimental $P_E(t)$ and the shifted harmonic $P_P(t)$ pressure pulsatile inputs, when pressure maxima and minima are the same (440 and 160 Pa respectively).

-As expected, CFD calculations with model $m(s)$ for the hematocrit field, give the same shear rate at the wall for any global hematocrit. The differences appear in this case moving away from the wall towards the vessel axis. So, in the framework of model $m(s)$ the permeability at the boundary layer is not significantly affected by local hematocrits. In the framework of model m with a nonzero hematocrit at the wall, the permeability is modified when the global hematocrit changes.

- With $\beta = 1$ the viscosity field given by equation (112) reduces to $\mu_{N,m(s)}(y) = \frac{\mu_p}{y^{m(s)}}$

A potential law formula like this was introduced by Womersley in equation (110) trying to obtain analytical solutions for oscillatory pressure pulses of any frequency. He found that for $m = 2$ and $m = 4$ it is possible to obtain closed form solutions in terms of known special functions of mathematical physics (Suárez-Ántola 1980).

-If quasi-steady conditions are not applicable to the haematocrit dynamics in an axisymmetric blood flow, the unsteady nonlinear diffusion equation (47) for the haematocrit should be solved, suitably coupled with the Navier-Stokes equation, for the geometries studied in the present work. However, when there is quasi-equilibrium in the hydrodynamic diffusion process, equation (88) shows that the hematocrit field can be considered as steady, at least approximately, as was done here for purposes of digital simulation.

-The hematocrit field of model m can be derived from quasi-steady q-adic velocity profiles if a generalized Newtonian macro-rheological model of viscosity is used to describe the relation between local viscosity and local hematocrit. Also, model m formula for the hematocrit field is obtained from Quemada’s non-Newtonian viscosity model, when the shear rates adjacent to the wall are an order of magnitude either smaller or greater than Quemada’s critical value. For intermediate values a generalization of model m formula is obtained (equation (79)) giving a time varying hematocrit if the flow is pulsatile. However, model m formula is not obtained from q-adic velocity profiles if Casson macro-rheological model is employed, except as an asymptotic zero order approximation when the shear stress adjacent to the wall is at least an order of magnitude greater than Casson's yield stress and Casson model reduces to a Newtonian model. This last result agrees with the fact that a q-adic profile can´t properly describe piston flow in a significant inner cylinder of flowing blood, although for q big enough the blunting of the velocity profile approaches a piston flow.

-Even without taking into account axial accumulation, the permeability k_{F-W} of the diffusive boundary layer may depend of the rheological model used. For quasi-steady axisymmetric tube flow, let us compare the consequences on the permeability of a given substance of employing the Newtonian and Casson models. The rheology independent wall shear stress τ_w will be taken to be the same in both models, and the asymptotic viscosity of the Casson model will be taken equal to the viscosity μ_N of the Newtonian model. Then, the wall shear rate according to the Casson model is $\dot{\gamma}_{w,C} = \frac{\left(\sqrt{\tau_w} - \sqrt{\tau_y}\right)^2}{\mu_N}$, and according to the Newtonian model $\dot{\gamma}_{w,N} = \frac{\tau_w}{\mu_N}$. From these equations it follows: $\sqrt{\dot{\gamma}_{w,C}} = \sqrt{\dot{\gamma}_{w,N}} - \sqrt{\frac{\tau_y}{\mu_N}}$ Then, for the same shear stress τ_w, $\dot{\gamma}_{w,C}$ is always less than $\dot{\gamma}_{w,N}$. The permeability is a strictly increasing function of $\dot{\gamma}_w$ (according to a simplified but often quoted model, it is proportional to $\sqrt[3]{\dot{\gamma}_w}$). As consequence, the fluid to wall permeability of a given substance, for the same τ_w, will be less if the fluid behaves like a Casson fluid, relative to a Newtonian fluid whose viscosity is equal to the asymptotic viscosity of the Casson fluid. This remark could be used to justify the calculation of the approximate fluid to wall permeability (of oxygen and other substances with a transport limit step in the boundary layer) from the digital simulation of the effect of blood viscosity on hemodynamic factors in a small, bifurcated artery, that appear in the work of Kanaris (Kanaris et al. 2012).

-The function $u_m(y) = -u_w \cdot y$ was derived by Scott applying a theoretical framework already developed by Chan and Leal to describe the motion of a single deformable particle suspended in a Newtonian fluid. For this derivation the particle was at a certain distance from the flow axis, immersed in the parabolic 2-adic velocity field corresponding to an already established steady axisymmetric low Reynolds number flow in a cylindrical tube. In principle, it can be applied to dilute enough suspensions. Nevertheless, Scott argued about the possibility of extending the derivation to concentrated suspensions "treating the surrounding particles as a smeared-out effective medium" (op. cit. page 46). In such a case, instead of the plasma viscosity, a measure of the suspension viscosity would be used and a q-adic velocity profile could be employed instead of the 2-adic one.

- Hydrodynamic diffusion allows an understanding of a mechanism of axial accumulation of formed elements, but this mechanism is dominant only in concentrated enough suspensions. In dilute suspensions other migration mechanisms can be dominant. Now, hydrodynamic diffusion is closely related with a stochastic approach to axial accumulation, like the already classical approach to mathematically model the spatial and temporal distribution in population dynamics (Suárez-Ántola 1979, Okubo 1980). However, as will be discussed elsewhere, this last approach can be formulated to embrace concentrate and dilute suspensions.

To end, summing up:

-Taking into account spatial variations of viscosity may modify significantly local hemodynamics and fluid-to-wall transport processes as well as pumping power needed to maintain pulsated flow in a small artery, both with (generalized) Newtonian and Non-Newtonian rheology.

-In the considered global (tube) haematocrit range (35-55%), obtained shear rate profiles and transport parameters in fluid adjacent to the wall are affected by the macro-rheological model used and by the local haematocrit field according to the micro-rheological model proposed.

(F) References:

Ames, W., *Numerical Methods for Partial Differential Equations*, Academic Press, Boston, 3rd edition,1992

Anastasiou A., Spyrogianni A., Koskinas K., Giannoglou G. and Paras S., Experimental investigation of the flow of a blood analogue fluid in a replica of a bifurcated small artery, *Medical Engineering & Physics* **34**, 211– 218, 2012

Baskurt O. et al. (Eds.), *Handbook of Hemorheology and Hemodynamics*, IOS Press, Amsterdam, 2007

Baskurt O. and Meiselman H., Hemodynamic effects of red blood cell aggregation, *Indian Journal of Experimental Biology* **45** 25-31, 2007

Bayliss L., The axial drift of the red cells when blood flows in a narrow tube, *J Physiol.*, **149**,593–613, 1959

Biasetti J., Spazzini P.G., Hedin U. and Gasser T.C., Synergy between shear-induced migration and secondary flows on red blood cells transport in arteries: considerations on oxygen transport, *J. R. Soc. Interface* **11**: 20140403, 2014

Caro C. et al., *The mechanics of circulation*, Cambridge University Press, Cambridge, UK, 2012

Chandran K., Rittgers S. and Yoganathan A., *Biofluid mechanics: the human* *circulation*, 2nd ed, CRC Press, Boca Raton, FL, 2012

Chen X., Tan K., Lam Y. and Chai J., The transverse particle migration of highly filled polymer fluid flow in a pipe, *Singapore-MIT Alliance (SMA)*, 2003 http://hdl.handle.net/1721.1/3757

Cokelet G. and Meiselman H., Macro and micro rheological properties of blood, in Baskurt O.K. et al. (Eds.), *Handbook of Hemorheology and Hemodynamics*, IOS Press, Amsterdam, 2007

Cokelet G. and Meiselman H., Basic aspects of hemorheology, in Baskurt O.K. et al. (Eds.), *Handbook of Hemorheology and Hemodynamics*, IOS Press, Amsterdam, 2007

COMSOL Multiphysics Reference Guide, Version: 4.2a, 2011

COMSOL Multiphysics User's Guide, Version: 4.3a, 2012

Cooney D.O., *Biomedical engineering principles*, Marcel Dekker, NY, 1976

Coppola G. and Caro C., Arterial geometry, flow pattern, wall shear and mass transport: potential physiological significance, *J. R. Soc. Interface* **6,** 519-528, 2009

Davis R., Hydrodynamic diffusion of suspended particles: a symposium, *J. Fluid Mech.*, **310**, 325-335, 1996

Dillon, P., *Biophysics: A physiological approach*, Cambridge University Press, Cambridge, UK, 2012

Gardiner, C., *Handbook of Stochastic Methods for Physics, Chemistry and the Natural Sciences*, Springer, Berlin, 2nd edition, 1986

Gershenfeld, N, *The nature of mathematical modeling*, Cambridge University Press, Cambridge, UK, 1999

Gidaspow D. and Huang J., Kinetic theory-based model for blood flow and its viscosity, *Annals of Biomedical Engineering* **37**, 1534-1545, 2009

Glaser, R., *Biophysics*, Springer, Berlin, 2001

Kanaris A., Anastasiou A. and Paras S., Modeling the effect of blood viscosity on hemodynamic factors in a small, bifurcated artery, *Chemical Engineering Science* **71**, 202–211, 2012

Lapasin R., Grassi M. and Pricl S., Rheological modeling of fractal and dense suspensions, *The Chemical Engineering Journal* **64**, 99-106, 1996

Lebon G., Jou D., and Casas-Vázquez J., *Understanding non-equilibrium thermodynamics: foundations, applications, frontiers*, Springer, Berlin, 2010

Lin C. and Segel L. *Mathematics Applied to Deterministic Problems in the Natural Sciences*, SIAM, Philadelphia, 1988

Matas J., Morris J., and Guazzelli E., Lateral forces on a sphere, *Oil & Gas Science and Tecnology*, 59 (1), 59-70, 2004

Merrill E. W., Rheology of Blood, *Physiological Reviews* **49**, 863-888, 1969

Nichols W., O'Rourke M. and Vlachopoulos Ch., *McDonald's blood flow in arteries: theoretical, experimental, and clinical principles*, Hodder-Arnold, London, UK, 2011

Okubo A., *Diffusion, and ecological problems: mathematical models*, Springer, Berlin, 1980.

Pearl J., *The effect of velocity on the electrical conductivity of blood*, M. Sc. Thesis in Electrical engineering, Newark College of Engineering, Newark, NJ, 1961

Phillips R., Armstrong R., Brown R., Graham A. and Abbot J., “A Constitutive Equation for Concentrated Suspensions that Accounts for Shear-induced Particle Migration,” *Phys. Fluids A* **4**, 30–40, 1992

Polyanin A. and A. Manshirov, *Handbook of mathematics for engineers and scientists*, CRC Press, Boca Raton, Florida, 2007

Popel, S. and Johnson, P., Microcirculation and hemorheology, *Annual Reviews of Fluid Mechanics,* **37**, 43-69, 2005

Quemada D., Rheology of concentrated disperse systems and minimum energy dissipation principle: I.Viscosity-concentration relationship, *Reol. Acta*, **16**, 82-94, 1977

Quemada D., Rheology of concentrated disperse systems: II A model for non-Newtonian shear viscosity in steady flow, *Reol. Acta*, **17**, 632-642, 1978 (a)

Quemada D., Rheology of concentrated disperse systems: III. General features of the proposed non-Newtonian model and comparison with experimental data, *Reol. Acta*, **17**, 643-653, 1978 (b)

Rampling M.W., History of hemorheology, in Baskurt O.K. et al. (Eds.), *Handbook of Hemorheology and Hemodynamics*, IOS Press, Amsterdam, 2007

Ross-Ethier C., Computational modeling of mass transfer and links to atherosclerosis, *Annals of Biomedical Engineering,* **30**, 461-471, 2002

Ross-Ethier, C. and Simmons C., *Introductory Biomechanics: From cells to organisms*, Cambridge University Press, Cambridge, UK, 2007

Scott M., *The modeling of Blood Rheology in small vessels,* Ph. D. Thesis in Applied

Mathematics, Waterloo University, Ontario, 2005

Shauly A., Wachs A. and Nir A., Shear-induced particle resuspension in settling polydisperse concentrated suspension, *International Journal of Multiphase Flow* **26**, 1-15, 2000

Slattery, J., *Momentum, energy and mass transfer in continua*, McGraw-Hill Kogakusha, Tokyo, 1972

Starov V., Zhdanov V., Meireles M. and Molle C., Viscosity of concentrated suspensions: influence of cluster formation, *Adv. Colloid Interface Sci*., **96** (1-3), 279-93, 2002

Suárez-Ántola R, *Stochastic Processes and Spatial Distributions of Biological Populations*, DPE, Universidad de la República, Montevideo, Uruguay, 1979

Suárez-Antola R., *Topics of macro and micro rheology of blood*, DPE, Universidad de la República, Montevideo, Uruguay, 1980

Suárez-Bagnasco D., Balay G., Cymberknop L., Armentano R.L. and Negreira C., In-vitro hemodynamic measurements and in-silico simulation of a physical model of arterial bifurcation, *J. Phys. Conf. Series* **477,** 2013

Tarbell J. and Qiu Y., Arterial wall mass transport, in Bronzino J. (Ed), *The biomedical engineering handbook*, Vol. 2, 3rd Ed., CRC, 2006

Taylor M., The flow of blood in narrow tubes: The axial stream and its formation, as determined by changes in optical density, *Aust J Exp Biol Med Sci*., **33(1)**,1–15, 1955

Taylor C. and Draney M., Experimental and computational methods in cardiovascular fluid mechanics, *Annu. Rev. Fluid Mech.* **36**, 197-231, 2004

Taylor C. and Humphrey J., Open Problems in Computational Vascular Biomechanics: Hemodynamics and Arterial Wall Mechanics, *Comp. Methods Appl. Mech. Eng.*,**198: (45-46)**, 3514–3523, 2009

van Dinther A., Schroën C., Imhof A., Vollebregt H., and Boom R., Flow-induced particle migration in microchannels for improved microfiltration processes, *Microfluid Nanofluid* **15**, 451-465, 2013

Woodcock J., Physical-properties of blood and their influence on blood-flow measurement, *Reports on Progress in Physics*, **39**(**1**), 65–127, 1976

Yilmaz F. and Gundogdu M., A critical review on blood flow in large arteries; relevance to blood rheology, viscosity models, and physiologic conditions, *Korea-Australia Rheology Journal*, **20**, 197-211, 2008

Zhao H., Shaqfeh E., and Narsimhan V., Shear induced particle migration and margination in a cellular suspension, *Physics of Fluids*, **24**, 011902 (1-21), 2012